Short Article

Cell Metabolism

# Inactivation of the Glucose-Dependent Insulinotropic Polypeptide Receptor Improves Outcomes following Experimental Myocardial Infarction

## Graphical Abstract

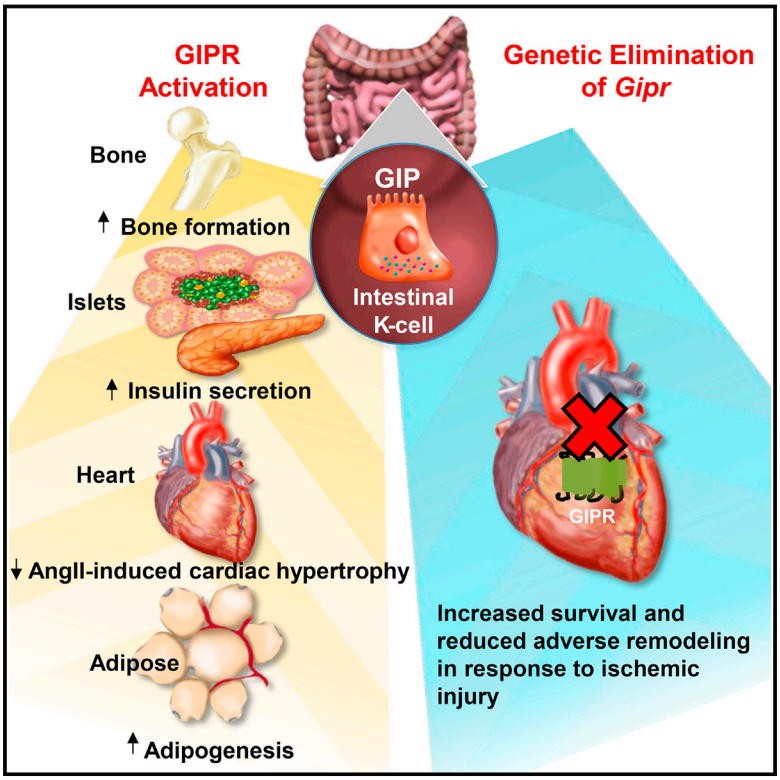


## Highlights

- GIP does not impair ventricular function or survival after ischemic cardiac injury
- Gain and loss of GIPR signaling regulates cardiac lipid metabolism
- Selective elimination of the cardiomyocyte GIPR protects against ischemic injury
- Cardiac GIPR expression is conserved in mouse and human ventricular cardiomyocytes

## Authors

John R. Ussher, Jonathan E. Campbell, Erin E. Mulvihill, ..., Yutaka Seino, Jinya Suzuki, Daniel J. Drucker

## Correspondence

drucker@lunenfeld.ca

## In Brief

Ussher et al. demonstrate that the GIP receptor is expressed in cardiomyocytes and that direct activation of GIPR signaling regulates cardiac lipid metabolism. GIPR agonism was not deleterious in the context of ischemic cardiac injury; however, germline- or cardiomyocyte-selective loss of GIPR signaling increased survival and reduced adverse ventricular remodeling.

Ussher et al., 2018, Cell Metabolism *27*, 450–460
February 6, 2018 
https://doi.org/10.1016/j.cmet.2017.11.003

CellPress

CellPress

Cell Metabolism
Short Article

# Inactivation of the Glucose-Dependent Insulinotropic Polypeptide Receptor Improves Outcomes following Experimental Myocardial Infarction

John R. Ussher,[1,2] Jonathan E. Campbell,[1,3] Erin E. Mulvihill,[1,6] Laurie L. Baggio,[1] Holly E. Bates,[1,8] Brent A. McLean,[1] Keshav Gopal,[2] Megan Capozzi,[3] Bernardo Yusta,[1] Xiemin Cao,[1] Safina Ali,[1] Minsuk Kim,[1,7] M. Golam Kabir,[1] Yutaka Seino,[4] Jinya Suzuki,[5] and Daniel J. Drucker[1,9,*]

[1]Lunenfeld Tanenbaum Research Institute, Mount Sinai Hospital, University of Toronto, Toronto, ON M5G 1X5, Canada
[2]Faculty of Pharmacy and Pharmaceutical Sciences, University of Alberta, Edmonton, AB T6G 2H7, Canada
[3]Duke Molecular Physiology Institute, Duke University Medical Center, Durham, NC 27701, USA
[4]Kansai Electric Power Hospital and Medical Research Institute, 2-1-7 Fukushima-ku, Osaka 553-0003, Japan
[5]Faculty of Medical Sciences, University of Fukui, Fukui 910-1193, Japan
[6]Present address: University of Ottawa Heart Institute, Ottawa, ON K1Y 4W7, Canada
[7]Present address: Ewha Womans University, Seodaemun-gu, Seoul 03760, Republic of Korea
[8]Present address: Trent University, Peterborough, ON K9J 7B8, Canada
[9]Lead Contact
*Correspondence: drucker@lunenfeld.ca
https://doi.org/10.1016/j.cmet.2017.11.003

## SUMMARY

**Incretin hormones exert pleiotropic metabolic actions beyond the pancreas. Although the heart expresses both incretin receptors, the cardiac biology of GIP receptor (GIPR) action remains incompletely understood. Here we show that GIPR agonism did not impair the response to cardiac ischemia. In contrast, genetic elimination of the *Gipr* reduced myocardial infarction (MI)-induced ventricular injury and enhanced survival associated with reduced hormone sensitive lipase (HSL) phosphorylation; it also increased myocardial triacylglycerol (TAG) stores. Conversely, direct GIPR agonism in the isolated heart reduced myocardial TAG stores and increased fatty acid oxidation. The cardioprotective phenotype in $Gipr^{-/-}$ mice was partially reversed by pharmacological activation or genetic overexpression of HSL. Selective *Gipr* inactivation in cardiomyocytes phenocopied $Gipr^{-/-}$ mice, resulting in improved survival and reduced adverse remodeling following experimental MI. Hence, the cardiomyocyte GIPR regulates fatty acid metabolism and the adaptive response to ischemic cardiac injury. These findings have translational relevance for developing GIPR-based therapeutics.**

## INTRODUCTION

Gut hormones are secreted in response to nutrient consumption and control gastrointestinal motility, nutrient digestion, absorption, and assimilation. The conserved glucoregulatory actions of glucagon-like peptide-1 receptor (GLP-1R) agonists and the favorable metabolic activity arising from inhibitors of dipeptidyl peptidase-4 (DPP-4) enabled the development of two new classes of incretin-based agents for the treatment of type 2 diabetes (T2D). The therapeutic importance of incretin therapies has been bolstered by the cardiovascular (CV) safety of DPP-4 inhibitors and by the reduced CV event rates shown for GLP-1R agonists (Drucker, 2016). These findings, together with cardioprotective actions of SGLT-2 inhibitors (Kaul, 2017), have increased interest in the cardiometabolic actions of investigational and established therapies for T2D and obesity.

There is now increased focus on the translational potential of next-generation metabolic therapies that improve GLP-1 action through addition of GIP receptor (GIPR) agonism (Tschöp et al., 2016). GIPR agonists, GIP-GLP-1 co-agonists, and unimolecular triple agonists incorporating GIPR agonism all produced substantial reductions in blood glucose and body weight in preclinical studies (Finan et al., 2015). Moreover, GIP-GLP-1 co-agonists reduced HbA1c and body weight in human subjects with T2D (Finan et al., 2013; Frias et al., 2017). The relevance of GIPR signaling for human metabolism is further underscored by the association of genetic variation within the human *GIPR* with body mass index, β cell function, cerebrovascular disease, and the risk of T2D (Berglund et al., 2016; Finan et al., 2016).

Although actions of glucagon and GLP-1 on the heart have been extensively studied, little is known about the cardiovascular biology of the GIPR. Here we show that GIPR agonism is not deleterious in normoglycemic mice with myocardial infarction (MI). Unexpectedly, $Gipr^{-/-}$ mice exhibited increased survival after sustained ischemic cardiac injury. Moreover, $Gipr^{CM-/-}$ mice with conditional inactivation of the *Gipr* in adult cardiomyocytes exhibited reduced infarct size and improved survival after MI. Furthermore, we demonstrate that GIPR signaling directly engages metabolic pathways controlling cardiac lipid metabolism. Collectively, these results reveal the biological importance of cardiomyocyte GIPR signaling in the context of ischemic cardiac injury. These findings have implications for development of GIP-based therapies for the treatment of metabolic disease.

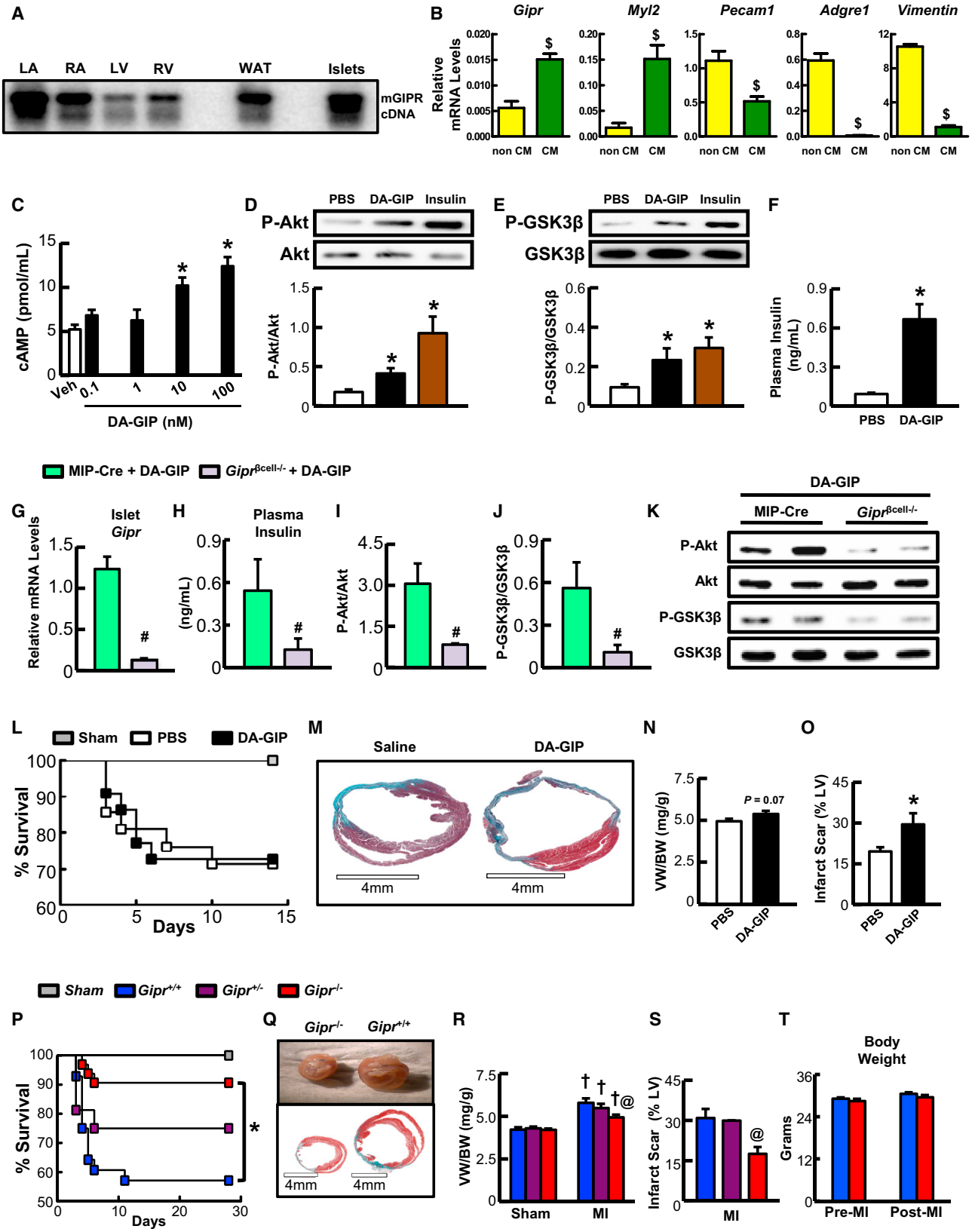


(legend on next page)

## RESULTS

### The *Gipr* Is Expressed in the Heart and Linked to Adenylate Cyclase Activation

A full-length *Gipr* mRNA transcript was identified in all four chambers of the mouse heart (Figure 1A) as well as in mouse neonatal cardiac myocytes and HL-1 atrial myocytes (Figures S1A and S1B). Evaluation of three different commercially available GIPR antisera revealed that they were unsuitable (problems with sensitivity or specificity) for detection of the mouse GIPR (Figure S1C). Consistent with transcriptomics data localizing *Gipr* to mouse cardiomyocytes (Quaife-Ryan et al., 2017), *in situ* hybridization identified a subset of *Gipr*-positive cardiac myocytes in the mouse ventricle and atrium (Figure S1D). *GIPR* mRNA transcripts were also detected in RNA from all four chambers of the human heart (Figure S1E). Moreover *Gipr* and *Myl2* mRNA transcripts were enriched in RNA from adult mouse ventricular cardiac myocyte fractions, whereas *Pecam1*, *Adgre1*, and *vimentin* mRNAs were more abundant in the non-cardiomyocyte fraction (Figure 1B). Consistent with the canonical GIPR signaling pathway, activation of the GIPR in HL-1 atrial myocytes increased cAMP levels (Figure 1C).

### Systemic GIPR Activation Does Not Modify the Outcome of Myocardial Ischemia-Induced Cardiac Injury

GIP stimulates insulin secretion and exhibits insulinomimetic activity, raising the possibility that GIP engages cardiac signal transduction through direct (cardiomyocyte GIPR), and indirect (insulin) mechanisms. Accordingly, we assessed myocardial insulin signaling pathways following peripheral administration of the degradation-resistant GIPR agonist [D-Ala$_2$]GIP (24 nmol/kg BW) or insulin (0.7 U/kg BW). [D-Ala$_2$]GIP increased Akt and glycogen synthase kinase 3β (GSK3β) phosphorylation in heart tissue from wild-type (WT) mice (Figures 1D and 1E), associated with increased levels of circulating insulin (Figure 1F). These cardiac actions of [D-Ala$_2$]GIP were extinguished in mice with β-cell-specific deletion of the *Gipr* (*Gipr*$^{\beta cell-/-}$) (Figures 1G–1K). Hence, interpretation of GIP action on the heart *in vivo* may be complicated by concomitant activation of cardiac signaling pathways through indirect (insulin-dependent) mechanisms.

We next studied GIPR activation in mice with permanent occlusion of the left anterior descending (LAD) coronary artery. One week pre-treatment with [D-Ala$_2$]GIP had no effect on mortality (Figure 1L); however, ventricular weights, reflecting remodeling, trended higher, ($p = 0.07$), and left ventricle (LV) scar formation was increased in hearts from [D-Ala$_2$]GIP-treated mice (Figures 1M–1O).

### *Gipr*$^{-/-}$ Mice Exhibit a Cardioprotective Response to Experimental Ischemia

We next determined whether loss of basal GIPR signaling impacts the response to ischemic cardiac injury. *Gipr*$^{-/-}$ mice with whole-body knockout of *Gipr* expression displayed normal cardiac function, heart rate, and structure in the basal state (Table S1). Unexpectedly, *Gipr*$^{-/-}$ mice exhibited improved survival (Figure 1P) and less adverse LV remodeling (Figures 1Q–1S) 4 weeks post-MI without changes in body weight (Figure 1T). An intermediate level of improved survival was observed in *Gipr*$^{+/-}$ mice (Figure 1P). This cardioprotection was not associated with changes in Akt, GSK3β, or AMPK phosphorylation (Figures 2A–2C). Although adipose triglyceride lipase (ATGL) protein expression was unchanged (Figure 2D), myocardial triacylglycerol (TAG) content was increased in *Gipr*$^{-/-}$ mice post-MI (Figure 2E), associated with decreased hormone-sensitive lipase (HSL) phosphorylation in viable *Gipr*$^{-/-}$ myocardium (Figures 2F and 2G). Furthermore, mediators of myocardial injury—including macrophage inflammatory factor-1 (MIF-1), secreted protein acidic and rich in cysteine (SPARC), caveolin-1, and angiotensin-converting enzyme 2 (ACE2)—remained unchanged

**Figure 1. Cardiac GIPR Expression and Action in the Normal and Ischemic Heart**

(A) *Gipr* expression in the mouse heart detected by RT-PCR; blot was hybridized with an oligonucleotide probe specific to the *Gipr* cDNA. *Gipr* mRNA transcripts were detected in all four heart chambers (left atria, LA; right atria, RA; left ventricle, LV; and right ventricle, RV). Epididymal white adipose tissue (WAT) and islet mRNA were used as controls.

(B) Real-time PCR demonstrating enrichment of *Gipr* and *Myl2* mRNA transcripts in cardiac myocyte (CM) fractions versus *Pecam1* (CD31), *Adgre1* (F4/80), and *vimentin* that were more abundant in noncardiac myocyte (non-CM) fractions from adult mouse hearts (n = 4).

(C) cAMP levels in HL-1 cells assessed 10 min after stimulation with [D-Ala$_2$]GIP (DA-GIP) (n = 5).

(D and E) Akt serine 473 phosphorylation (60 kDa) (D) and GSK3β serine 9 phosphorylation (46 kDa) (E) in hearts from overnight fasted mice treated with PBS or DA-GIP (24 nmol/kg body weight) for 1 hr (n = 4 or 5).

(F) Plasma insulin levels in overnight fasted mice treated with PBS, DA-GIP (24 nmol/kg body weight), or insulin (0.7 U/kg body weight) for 1 hr (n = 4 or 5).

(G) *Gipr* mRNA levels in islets from MIP-Cre and *Gipr*$^{\beta cell-/-}$ mice following 5 days of tamoxifen treatment (n = 4 or 5).

(H) Plasma insulin levels in overnight fasted MIP-Cre and *Gipr*$^{\beta cell-/-}$ mice treated with DA-GIP (24 nmol/kg body weight) (n = 4 or 5).

(I and J) Akt serine 473 phosphorylation (60 kDa) (I) and (J) GSK3β serine 9 phosphorylation (46 kDa) (J) in overnight fasted MIP-Cre and *Gipr*$^{\beta cell-/-}$ mice treated with DA-GIP (24 nmol/kg body weight) (n = 3–5).

(K) Representative images for western blot data quantified in (I) and (J).

(L) MI-induced mortality in PBS and DA-GIP-treated C57BL/6J mice (n = 19–21).

(M) Representative images depicting LV structure and infarct scar formation 2 weeks post-MI.

(N and O) Ventricular weight:body weight (VW/BW) ratios (n = 9 or 10) (N) and LV infarct scar formation (O) in PBS and DA-GIP treated C57BL/6J mice (n = 7 or 8).

(P) Mortality in *Gipr*$^{+/+}$, *Gipr*$^{+/-}$, and *Gipr*$^{-/-}$ mice subjected to permanent LAD coronary artery occlusion (n = 16–32).

(Q) Representative images depicting LV structure and scar formation 4 weeks post-MI.

(R and S) Ventricular weight:body weight (VW/BW) ratios (n = 5–12) (R) and LV infarct scar formation (S) in *Gipr*$^{+/+}$ and *Gipr*$^{-/-}$ mice (n = 7 or 8).

(T) Body weights in *Gipr*$^{+/+}$ and *Gipr*$^{-/-}$ mice pre- and post-permanent LAD coronary artery occlusion surgery (n = 9–12).

Values represent mean ± SE. Differences were determined using a Kaplan Meier survival analysis, an unpaired Student's two-tailed t test, or a 1-way or 2-way ANOVA followed by a Bonferroni post hoc analysis. $^{\$}p < 0.05$, significantly different from non-cardiomyocyte; $^{*}p < 0.05$, significantly different from PBS/vehicle (Veh) control; $^{\#}p < 0.05$, significantly different from MIP-Cre + DA-GIP; $^{\dagger}p < 0.05$, significantly different from sham counterpart; $^{@}p < 0.05$, significantly different from *Gipr*$^{+/+}$.

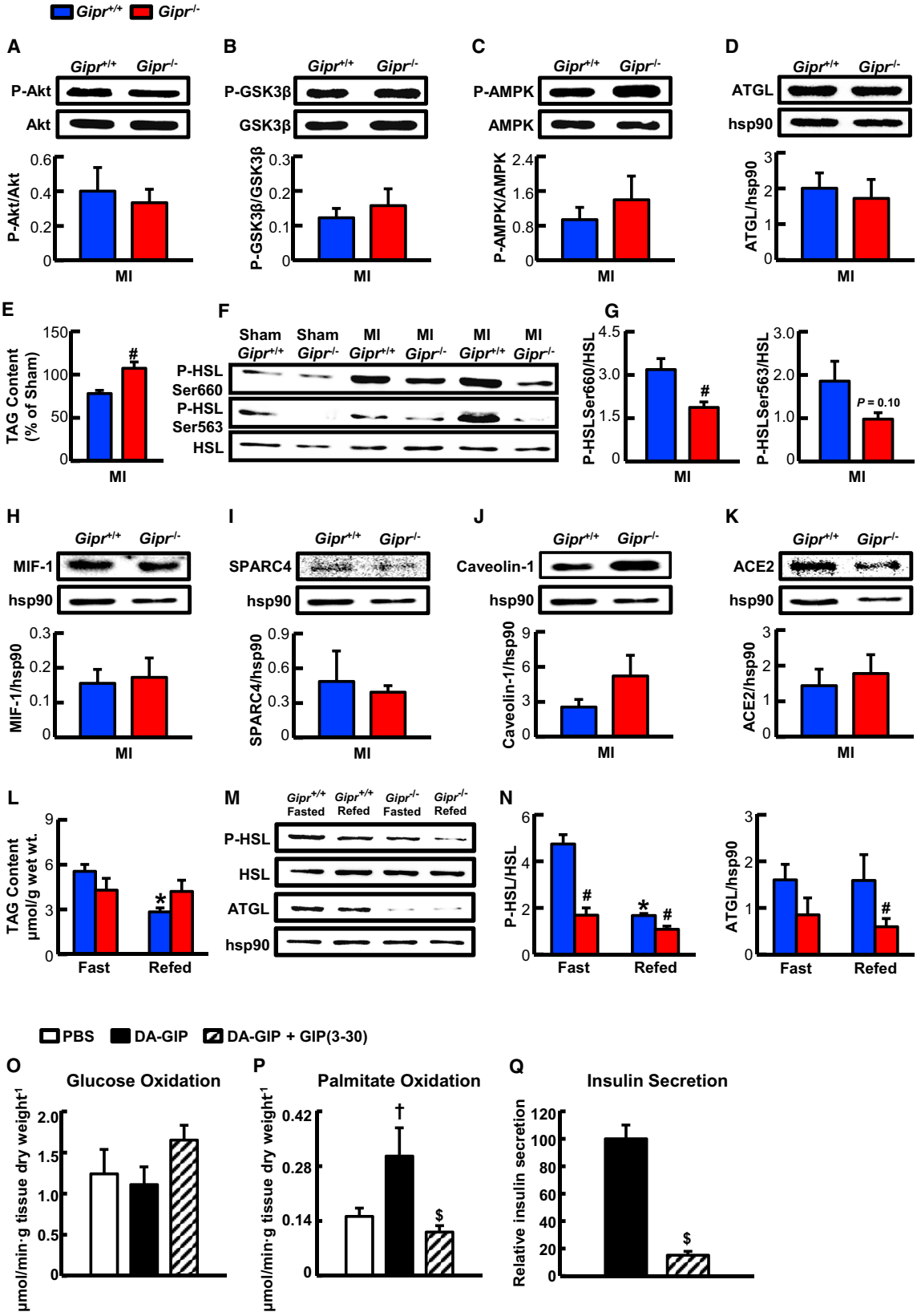


(legend on next page)

(Figures 2H–2K). Moreover, ventricular mRNA transcript levels of genes regulating extracellular matrix (ECM) remodeling, inflammation, or apoptosis were not different between *Gipr*$^{+/+}$ versus *Gipr*$^{-/-}$ mice post-MI (Figures S1F–S1H), with the exception of X-linked inhibitor of apoptosis protein (*Birc4*), which was elevated in *Gipr*$^{-/-}$ mice hearts (Figure S1H). Likewise, mRNA expression of PPARα, PPARα target genes, and fetal reprogramming genes was comparable in hearts from *Gipr*$^{+/+}$ and *Gipr*$^{-/-}$ mice (Figures S1I and S1J). In further support of a link between myocardial GIPR signaling and TAG metabolism, refeeding reduced myocardial TAG content in *Gipr*$^{+/+}$ but not in *Gipr*$^{-/-}$ hearts (Figure 2L) in association with a reduction in HSL phosphorylation and ATGL protein expression in *Gipr*$^{-/-}$ hearts (Figures 2M and 2N).

We next examined whether GIPR signaling in the heart directly controls TAG/fatty acid metabolism by perfusing working mouse hearts aerobically with either vehicle or [D-Ala$_2$]GIP. GIPR activation had no effect on myocardial glucose oxidation, but it increased fatty acid oxidation rates (Figures 2O and 2P). Moreover, the GIP antagonist GIP(3-30) (Sparre-Ulrich et al., 2017), which attenuated GIP-stimulated insulin secretion in islets (Figure 2Q), completely abrogated the increase in myocardial fatty acid oxidation rates (Figure 2P).

## GIPR Deficiency Does Not Confer Protection against Experimental Heart Failure

Despite exhibiting robust protection against ischemic cardiac injury, *Gipr*$^{-/-}$ mice did not exhibit improved survival in response to doxorubicin-induced cardiac toxicity (Figure S2A), though cardiac atrophy was attenuated (Figures S2B and S2C) and myocardial HSL phosphorylation was unaltered (Figure S2D). Similarly, LV function was not improved in *Gipr*$^{-/-}$ mice following transverse aortic-constriction-induced heart failure (Figures S2E and S2F). Hence, the cardioprotection elicited by reduced cardiac GIPR activity appears specific to the context of ischemic injury.

## GIPR Activation Directly Increases Cardiac HSL Phosphorylation and Modulates TAG Content

We next determined whether reduced HSL phosphorylation in *Gipr*$^{-/-}$ hearts reflects changes in cardiac GIPR signaling. HSL phosphorylation was increased in Langendorff-perfused mouse hearts and in HL-1 cells directly treated with [D-Ala$_2$]GIP (Figures 3A and 3B). Moreover, intracellular TAG content was reduced following [D-Ala$_2$]GIP treatment in oleic-acid-loaded HL-1 cells (Figure 3C), whereas a ~60% siRNA-mediated reduction of HSL protein expression in HL-1 cells (Figure 3D) attenuated the [D-Ala$_2$]GIP-mediated decrease in intracellular TAG content (Figure 3E).

## GIP-Induced HSL Phosphorylation Depends on Protein Kinase G/Extracellular-Signal-Regulated Kinase (ERK) Activity

The GIPR-mediated increase in HSL phosphorylation in HL-1 cardiac myocytes was not prevented by the protein kinase A inhibitor H89, the cAMP antagonist Rp-cAMP (Figure S2G), or the p38 MAPK inhibitor SB203580 (Figure S2H). Forskolin increased HSL phosphorylation, which was blocked by H-89; however Epac2 activation with ESCA-AM did not enhance HSL phosphorylation (Figure S2I). In contrast, pretreatment with the MEK inhibitor U0126 abolished the [D-Ala$_2$]GIP-induced increase in HSL phosphorylation and the subsequent decrease in intracellular TAG content (Figures S2J and S2K). Moreover, [D-Ala$_2$]GIP increased ERK phosphorylation prior to changes in HSL phosphorylation (Figures S2L and S2M). The protein kinase G (PKG) activator 8-Br-cGMP increased ERK (Figure S3A) and HSL (Figure S3B) phosphorylation in a temporal pattern mimicking that seen following GIPR activation. Furthermore, pretreatment with U0126 abolished the 8-Br-cGMP-induced increase in ERK and HSL phosphorylation and the subsequent decrease in intracellular TAG content (Figures S3C and S3D). Similarly, treatment with [D-Ala$_2$]GIP increased phosphorylation of the PKG downstream target vasodilator-stimulated phosphoprotein (VASP), while pretreatment with the PKG inhibitor Rp-8-Br-cGMPS prevented both the GIPR-mediated increase in HSL, ERK, and VASP phosphorylation and the subsequent decrease in intracellular TAG content (Figures S3E–S3H).

## Pharmacological Activation or Cardiac Overexpression of HSL Partially Reverses the Cardioprotection against Ischemic Injury in *Gipr*$^{-/-}$ Mice

Phosphorylation of HSL is controlled by β-adrenergic signaling, and the $\beta_3$ adrenoceptor has the least promiscuous tissue

**Figure 2. GIPR Signaling Alters HSL Phosphorylation and Triglyceride Metabolism**

(A–D) (A) Akt phosphorylation at serine 473 (60 kDa), (B) GSK3β phosphorylation at serine 9 (46 kDa), (C) AMPK phosphorylation at threonine 172 (62 kDa), and (D) ATGL (54 kDa) protein expression in *Gipr*$^{+/+}$ and *Gipr*$^{-/-}$ mice hearts (viable myocardium) at 48 hr post-LAD coronary artery occlusion (MI) (n = 4 or 5).

(E) Triacylglycerol (TAG) content in hearts (viable myocardium) from *Gipr*$^{+/+}$ and *Gipr*$^{-/-}$ mice 48 hr post-LAD coronary artery occlusion as a percentage of sham *Gipr*$^{+/+}$ and *Gipr*$^{-/-}$ mice hearts (n = 5).

(F and G) Representative western blot images (F) and quantification (G) of HSL serine 660 and 563 phosphorylation (81–83 kDa) in hearts (viable myocardium) from *Gipr*$^{+/+}$ and *Gipr*$^{-/-}$ mice at 48 hr post-LAD coronary artery occlusion or sham surgery (n = 5 or 6).

(H–K) (H) MIF-1 (13 kDa) protein expression, (I) SPARC4 (42 kDa) protein expression, (J) Caveolin-1 (24 kDa) protein expression, and (K) ACE2 (~120–135 kDa) protein expression in *Gipr*$^{+/+}$ and *Gipr*$^{-/-}$ mice hearts (viable myocardium) at 48 hr post-LAD coronary artery occlusion (n = 4 or 5).

(L) Myocardial TAG content in *Gipr*$^{+/+}$ and *Gipr*$^{-/-}$ mice following a 24-hr fast or a 24-hr fast and 2-hr refeed (n = 4 or 5).

(M and N) Representative western blot images (M) and quantification (N) of HSL serine 660 phosphorylation (81–83 kDa) and ATGL (54 kDa) protein expression in hearts from both 24-hr-fasted and 24-hr-fasted and 2-hr-refed *Gipr*$^{-/-}$ mice and *Gipr*$^{+/+}$ littermates (n = 4 or 5).

(O and P) Glucose oxidation rates (O) and palmitate oxidation rates (P) in hearts aerobically perfused for 80 min and treated with either PBS or 20 nM [D-Ala$_2$]GIP (DA-GIP) at 45 min of perfusion (n = 4–7).

(Q) Suppression of DA-GIP (1 nM)-stimulated insulin secretion by GIP(3-30) (1 μM) in isolated, perifused islets from WT mice. (n = 3).

Values represent mean ± SE. Differences were determined using an unpaired Student's two-tailed t test or a 1-way or 2-way ANOVA followed by a Bonferroni post hoc analysis. $^{\#}p < 0.05$, significantly different from *Gipr*$^{+/+}$ counterpart; $^{*}p < 0.05$, significantly different from fasted counterpart; $^{\dagger}p < 0.05$, significantly different from PBS-treated; $^{\$}p < 0.05$, significantly different from DA-GIP-treated.

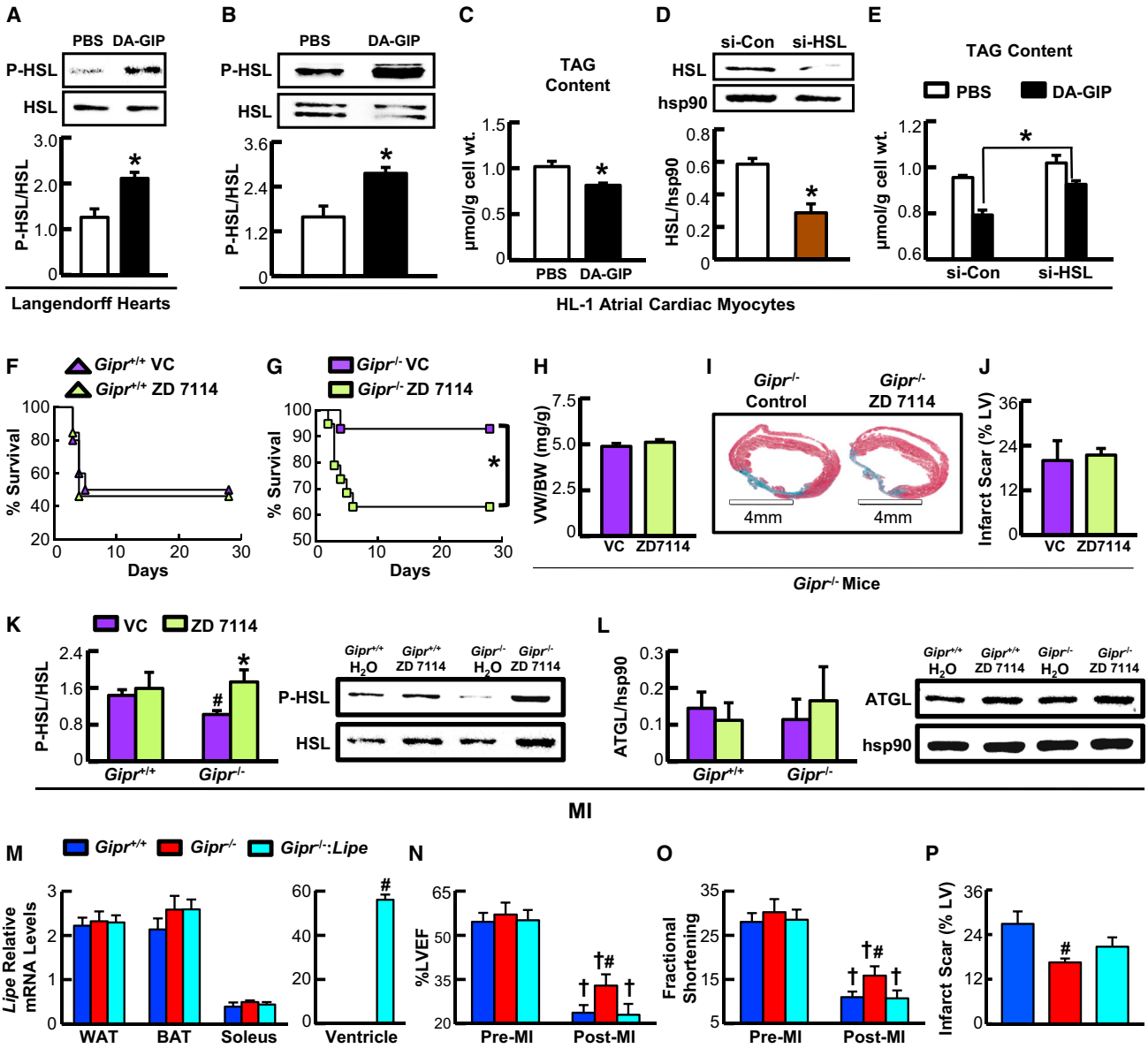


**Figure 3. GIPR Activation in Cardiac Myocytes Is Linked to HSL Phosphorylation, and Cardiac HSL Expression Partially Reverses the Cardioprotection Observed in *Gipr*$^{-/-}$ Mice**

(A and B) HSL serine 660 phosphorylation (81–83 kDa) in isolated perfused Langendorff mouse hearts (PBS or 20 nM DA-GIP for 20 min, n = 4 or 5) (A) and HL-1 cells (PBS or 100 nM DA-GIP for 3 hr, n = 5–7) (B).

(C) Intracellular triacylglycerol (TAG) content in HL-1 cells lipid-loaded with 0.4 mM oleic acid bound to 2% BSA for 16 hr followed by treatment with 100 nM DA-GIP for 4 hr (n = 4).

(D) HSL (81–83 kDa) protein expression in HL-1 cells treated with either scrambled (si-Con) or HSL-targeting (si-HSL) siRNA (n = 4 or 5).

(E) In HL-1 cells treated with either si-Con or si-HSL siRNA, intracellular TAG content was determined following lipid-loading with 0.4 mM oleic acid bound to 2% BSA for 16 hr prior to treatment with 100 nM DA-GIP for 4 hr (n = 4 or 5).

(F and G) MI-induced mortality in vehicle control (VC) and ZD 7114 (10 mg/kg, twice daily)-treated *Gipr*$^{+/+}$ (F) and *Gipr*$^{-/-}$ (G) mice (n = 12–19).

(H–J) Ventricular weight:body weight (VW:BW) ratios (H), left ventricle (LV) structure (I), and percent LV infarct scar (J) in VC and ZD 7114 (10 mg/kg, twice daily for 1 week immediately following LAD coronary artery occlusion)-treated *Gipr*$^{-/-}$ mice (n = 4–7) 4 weeks after permanent LAD coronary artery occlusion.

(K and L) HSL serine 660 phosphorylation (81 – 83 kDa) (K) and ATGL (54 kDa) protein expression (L) in infarcted hearts (viable myocardium) from VC and ZD 7114 (10 mg/kg, twice daily for 1 week immediately following LAD coronary artery occlusion)-treated *Gipr*$^{+/+}$ and *Gipr*$^{-/-}$ mice (n = 4 or 5).

(M) mRNA expression of *Lipe* in epididymal white adipose tissue (WAT), brown adipose tissue (BAT), soleus muscle, and ventricles from *Gipr*$^{+/+}$, *Gipr*$^{-/-}$, and *Gipr*$^{-/-}$:MHC-*Lipe* mice (n = 3–5).

(N and O) Percent left ventricular ejection fraction (LVEF) (N) and percent fractional shortening (O) in *Gipr*$^{+/+}$, *Gipr*$^{-/-}$, and *Gipr*$^{-/-}$:MHC-*Lipe* mice pre-MI and 1 week post-MI (n = 6–10).

*(legend continued on next page)*

distribution; it is predominantly restricted to cardiomyocytes, skeletal muscle, the urinary bladder, and adipose tissue. Administration of the selective $\beta_3$ adrenoceptor agonist ZD 7114 (10 mg/kg i.p.) increased myocardial HSL phosphorylation in WT mice 6 hr post-treatment (Figure S3I). ZD 7114 had no effect on ischemia-induced mortality following LAD coronary artery occlusion in *Gipr*$^{+/+}$ mice (Figure 3F). In contrast, ZD 7114 treatment increased mortality in *Gipr*$^{-/-}$ mice following LAD coronary artery occlusion (Figure 3G) in the absence of changes in body weight (Figure S3J) and independent of any changes in ischemia-induced adverse LV remodeling (Figures 3H–3J). HSL phosphorylation was increased (and ATGL expression unchanged) 48 hr post-MI in the viable myocardium of ZD 7114-treated *Gipr*$^{-/-}$ but not *Gipr*$^{+/+}$ mice (Figures 3K and 3L).

To determine whether reduced cardiac HSL activity contributed to the cardioprotective phenotype in *Gipr*$^{-/-}$ mice, we crossed mice overexpressing HSL (*Lipe*) in cardiac myocytes (Ueno et al., 2008) with *Gipr*$^{-/-}$ mice to generate *Gipr*$^{-/-}$:MHC-*Lipe* mice. Increased cardiac HSL expression in *Gipr*$^{-/-}$:MHC-*Lipe* mice (Figure 3M) did not reverse the improved survival observed in *Gipr*$^{-/-}$ mice post-MI (data not shown). However, the improved LV function observed in *Gipr*$^{-/-}$ mice 1 week post-MI was completely attenuated in *Gipr*$^{-/-}$:MHC-*Lipe* mice (Figures 3N and 3O, Table S1). Furthermore, LV infarct scar formation was no longer reduced in *Gipr*$^{-/-}$:MHC-*Lipe* mice (Figure 3P). Levels of MIF-1, SPARC4, caveolin-1, and ACE2 protein were unaltered in the viable myocardium of *Gipr*$^{-/-}$:MHC-*Lipe* mice 48 hr post-MI (Figures S3K and S3L).

### Cardiomyocyte-Selective Inactivation of the *Gipr* Attenuates Ischemia-Induced Mortality and Adverse LV Remodeling

We next assessed *Gipr* expression in right and left ventricles and the LV infarct zone after induction of MI. Remarkably, levels of *Gipr* mRNA transcripts were robustly yet transiently induced in the LV infarct zone by 12 and 24 hr after coronary artery ligation, returning to control levels by 48 hr (Figure 4A). To elucidate whether cardioprotection in *Gipr*$^{-/-}$ mice reflects selective GIPR deficiency in the myocardium, we conditionally inactivated the *Gipr* in adult mouse cardiomyocytes (*Gipr*$^{CM-/-}$). Cardiac *Gipr* mRNA expression was reduced by ~90%, with no changes in levels of *Gipr* mRNA in pancreas or white adipose tissue (Figure 4B). Strikingly, *Gipr*$^{CM-/-}$ mice exhibited enhanced survival and reduced adverse LV remodeling following LAD coronary artery occlusion (Figures 4C–4F). Consistent with observations in *Gipr*$^{-/-}$ mice, *Gipr*$^{CM-/-}$ mice also exhibited increased myocardial TAG content 48 hr post-MI (Figure 4G). Moreover, HSL phosphorylation was decreased in the viable myocardium 48 hr post-MI in *Gipr*$^{CM-/-}$ mice, reflecting a reduction in HSL protein expression (Figures 4H–4L). Collectively, findings in *Gipr*$^{CM-/-}$ mice substantially phenocopy the cardioprotective phenotype arising in whole-body *Gipr*$^{-/-}$ mice, revealing a role for the cardiomyocyte GIPR in the response to ischemic cardiac injury.

## DISCUSSION

Proglucagon-derived peptides—specifically, glucagon, GLP-1, and GLP-2—exert important actions in the control of energy metabolism, and their receptors represent validated targets for the treatment of metabolic and intestinal disease. Notably, activation of the GLP-1R is broadly cardioprotective in preclinical studies, and several GLP-1R agonists reduced the development of cardiovascular events, including rates of MI, in human subjects with T2D (Drucker, 2016; Kaul, 2017). Surprisingly, however, the available data localizes GLP-1R expression predominantly to the atrium—specifically, the sinoatrial node (Kim et al., 2013; Pyke et al., 2014). Hence, the mechanisms linking GLP-1R signaling to ventricular function and cardioprotection remain incompletely understood.

Although less extensively studied, the incretin hormone GIP and its receptor, GIPR, represent important components of a gut-islet axis controlling glucose homeostasis. GIP, together with GLP-1, mediates the glucoregulatory actions of DPP-4 inhibitors (Hansotia et al., 2004), medicines widely used to treat T2D. Clinical observations demonstrating restoration of glucoregulatory responses to GIP following a brief period of improved glucose control in human subjects with T2D (Højberg et al., 2009) have boosted enthusiasm for the therapeutic potential of GIPR agonism. Coagonists targeting the GIPR are under clinical investigation for the treatment of T2D (Finan et al., 2013; Frias et al., 2017), and daily administration of a unimolecular acylated GIP/GLP-1 dual agonist reduced HbA1c, cholesterol, and body weight over 12 weeks in metformin-treated subjects (Frias et al., 2017).

The efficacy of GIPR antagonism or reduction of GIP secretion for the treatment of obesity and its complications is also being explored (Campbell and Drucker, 2013; Finan et al., 2016). Genetic reduction of GIP secretion reduced adipose tissue mass and decreased body weight gain in high-fat-fed mice (Nasteska et al., 2014). Notably, acute GIPR antagonism reduced C-peptide levels and decreased adipose tissue uptake of fatty acids and triglyceride deposition in humans (Asmar et al., 2017), consistent with the hypothesis that sustained GIPR antagonism may prevent accretion of adipose tissue. Here we highlight a role for GIP action in the cardiovascular system, supported by demonstration that the GIPR gene is expressed in both the mouse and human heart. In contrast to the predominantly atrial expression of the *Glp1r* (Kim et al., 2013; Pyke et al., 2014; Quaife-Ryan et al., 2017), *Gipr* mRNA transcripts are detectable within ventricular myocytes. Moreover, expression of the mouse cardiac GIPR is transiently induced following ischemic cardiac injury, and functionally linked to control of lipid metabolism.

Physiologically, GIPR signaling also controlled HSL phosphorylation and myocardial TAG metabolism during meal intake. Moreover, we observed a GIPR-mediated reduction of TAG content in the isolated working heart (Figure S3M), and using radiolabeled tracers to measure myocardial metabolism, we

(P) LV infarct scar formation (percent of LV) in *Gipr*$^{+/+}$, *Gipr*$^{-/-}$, and *Gipr*$^{-/-}$:MHC-*Lipe* mice at 28 days post-MI (n = 7–11).

Values represent mean ± SE. Differences were determined using a Kaplan Meier survival analysis, an unpaired Student's two-tailed t test, or a 1-way or 2-way ANOVA followed by a Bonferroni post hoc analysis. *$p < 0.05$, significantly different from PBS, si-Con, or VC-treated counterpart; $^{\#}p < 0.05$, significantly different from *Gipr*$^{+/+}$ counterpart; $^{\dagger}p < 0.05$, significantly different from Pre-MI counterpart.

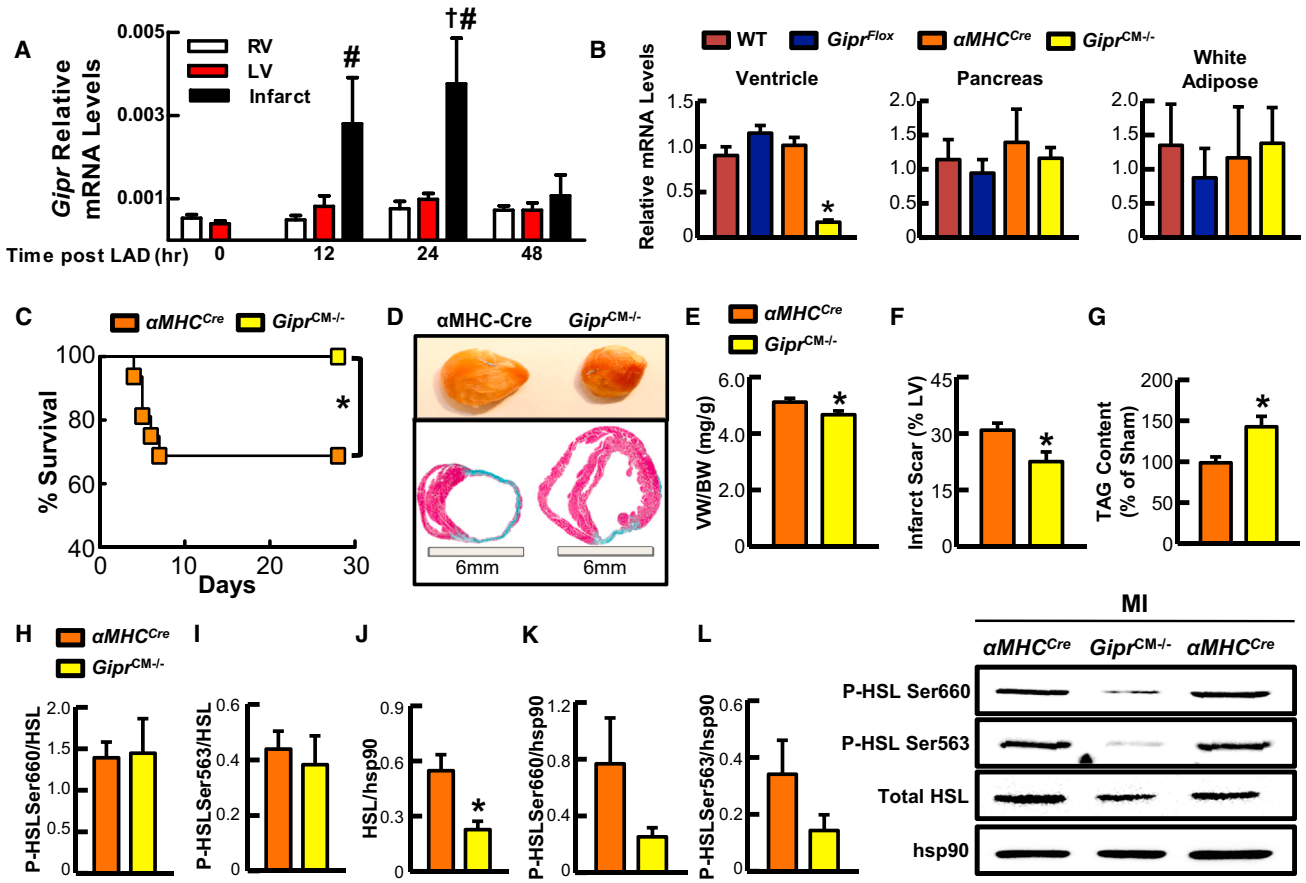


**Figure 4. Cardiomyocyte-Selective Inactivation of the *Gipr* Protects against Ischemia-Induced Mortality and Adverse LV Remodeling**

(A) *Gipr* mRNA expression in right ventricle (RV), left ventricle (LV) free wall, and LV infarct region from mice with no surgery (0) and 12, 24, and 48 hr after left anterior descending coronary artery (LAD) ligation (n = 6).

(B) *Gipr* mRNA expression in the ventricle, pancreas, and epididymal white adipose tissue of $Gipr^{CM-/-}$ mice and control littermates 5 weeks after completion of tamoxifen injections (n = 3–7).

(C) Mortality in αMHC-Cre and $Gipr^{CM-/-}$ mice subjected to permanent LAD coronary artery occlusion (n = 16 or 17).

(D) Representative images depicting LV structure and infarct formation 4 weeks after permanent LAD coronary artery occlusion.

(E and F) Ventricular weight:body weight (VW:BW) ratios (n = 9) (E) and LV infarct scar formation (percent of LV) (F) in αMHC-Cre and $Gipr^{CM-/-}$ mice at day 28 post-LAD coronary artery occlusion (n = 6).

(G) Triacylglycerol (TAG) content in hearts from αMHC-Cre and $Gipr^{CM-/-}$ mice 48 hr post-LAD coronary artery occlusion as a percentage of sham αMHC-Cre and $Gipr^{CM-/-}$ mice hearts (n = 3 or 4).

(H–L) HSL serine 660 (H and K) and 563 (I and L) phosphorylation (81–83 kDa) and HSL (81–83 kDa) protein expression (J) in hearts from infarcted (viable myocardium) αMHC-Cre and $Gipr^{CM-/-}$ mice (n = 5 or 6).

Values represent mean ± SE. Differences were determined using a Kaplan Meier survival analysis, an unpaired Student's two-tailed t test, or a 1-way ANOVA followed by a Bonferroni post hoc analysis. $^{\#}p < 0.05$, significantly different from LV at time 0; $^{\dagger}p < 0.05$, significantly different from RV and LV 24 hr post LAD; $^{*}p < 0.05$, significantly different from αMHC-Cre mice.

demonstrated that GIPR activation increases myocardial fatty acid oxidation rates. Our isolated working heart perfusions involved a 45-min equilibration period in order to saturate the TAG pool with radiolabeled palmitate. Hence, the decreased TAG content combined with a similar percentage of radiolabeled palmitate within the TAG pool 35 min post-GIPR activation (Figure S3N) suggests that GIPR activation in the heart is likely increasing both endogenous and exogenous fatty acid oxidation. Since previous studies have demonstrated that virtually all palmitate released within endogenous TAGs is oxidized via the isolated working heart, which is necessary to fuel the heart's enormous metabolic demand (Lopaschuk et al., 2010), it is unlikely that the TAG-released palmitate following cardiac GIPR activation would be liberated into the perfusate. Importantly, the cardioprotective phenotype arising in whole-body $Gipr^{-/-}$ mice was substantially reproduced by selective inactivation of the cardiomyocyte *Gipr*. Hence, reduction of cardiac GIPR activity represents a potential strategy for preservation of vulnerable myocardium in the context of ischemic heart disease.

GIP is known to enhance lipoprotein lipase and HSL activity in adipocytes (Asmar et al., 2017; Eckel et al., 1979; Timper et al., 2013), and GIP administration acutely enhanced pancreatic lipase activity in rats *in vivo* (Duan and

Erlanson-Albertsson, 1992). Here we extend these metabolic findings by demonstrating that gain and loss of GIPR signaling controls cardiac HSL activity. Hence, refeeding-associated increases in plasma GIP levels activate myocardial HSL to allow mobilization of endogenous TAG stores for energy metabolism, which may contribute to endogenous myocardial TAG stores accounting for ~25% of myocardial energy metabolism in humans subjected to hyperglycemia (Wisneski et al., 1990). Notably, the ischemia-associated increase in cardiac HSL phosphorylation was attenuated in *Gipr*$^{-/-}$ mice and increased following treatment with the $\beta_3$ adrenoceptor agonist, ZD 7114, associated with impaired survival following induction of MI. Moreover, cardiac-specific overexpression of HSL in *Gipr*$^{-/-}$ mice reversed the improved LV function and reduction in LV infarct scar formation observed in *Gipr*$^{-/-}$ mice post-MI. These findings suggest that reduction in HSL activity partially contributes to the cardioprotective phenotype of *Gipr*$^{-/-}$ mice. Nevertheless, selective genetic augmentation of cardiac HSL activity in *Gipr*$^{-/-}$:MHC-*Lipe* mice did not change survival or fully reverse the cardioprotective phenotype of *Gipr*$^{-/-}$ mice, so additional mechanisms beyond HSL are likely involved.

Taken together, our findings illustrate that reduction of cardiac GIPR expression is linked to impaired HSL-mediated control of TAG metabolism and marked cardioprotection against ischemic-induced myocardial injury. In contrast, GIPR agonism in the context of experimental ischemia was not associated with maladaptive cardiac responses or changes in survival. These findings inform the preclinical safety of GIPR agonism for the treatment of metabolic disease (Finan et al., 2013; Frias et al., 2017; Tschöp et al., 2016). The increasing interest in development of metabolic therapies that enhance GIP action (Campbell and Drucker, 2013; Finan et al., 2016), together with ongoing efforts to develop GIP receptor antagonists for the treatment of obesity, highlight the translational implications of the current findings. Our data reveals an entirely new aspect of GIP action in the heart, suggesting that attenuation of GIPR signaling in cardiomyocytes merits exploration as a potential strategy to mitigate ischemic cardiac injury.

### Study Limitations

The striking cardioprotective phenotype evident in *Gipr*$^{-/-}$, *Gipr*$^{+/-}$, and *Gipr*$^{CM-/-}$ mice strongly links reduction of cardiomyocyte GIPR signaling to attenuation of ischemic injury and adverse LV remodeling within the context of the cardiac ischemia model studied herein.

Nevertheless, these experiments have several limitations. The current studies characterizing the cardiac actions of the GIPR are confined to chronic ischemic-injury-induced heart failure and adverse LV remodeling, and it will be important to determine whether such actions are conserved in the setting of acute MI and transient ischemia/reperfusion (I/R) injury. Furthermore, ventricular remodeling was examined 4 weeks after ischemic injury in the current studies, and it will be useful to understand the impact ensuing from loss of cardiac GIPR signaling on remodeling at more chronic time points several months after myocardial infarction. Of interest, myocardial fatty acid oxidation rates are increased in subjects with obesity or diabetes and associated with poor cardiac recovery during I/R injury (Lopaschuk et al., 2010). As circulating GIP levels are increased in obesity (Jones et al., 1989), it is possible that increased cardiac GIPR signaling contributes to the elevated fatty acid oxidation rates and lipotoxicity associated with obesity-related cardiomyopathy and may exacerbate I/R injury in such scenarios. Moreover, whether reduced cardiac GIPR signaling influences the extent and consequences arising from MI within hours to days following LAD coronary artery occlusion requires investigation. Because we did not perform serial assessments of cardiac function post-MI for prolonged periods of time, we are precluded from understanding the chronic dynamic consequences of manipulating GIPR signaling in the setting of experimental MI. Our findings linking reduction of GIPR signaling to ischemic cardioprotection advance our understanding of incretin biology in the heart and raise new questions surrounding the cardiovascular importance of GIPR signaling in the normal and diseased heart.

## STAR★METHODS

Detailed methods are provided in the online version of this paper and include the following:

- KEY RESOURCES TABLE
- CONTACT FOR REAGENT AND RESOURCE SHARING
- EXPERIMENTAL MODEL AND SUBJECT DETAILS
  - Animal Husbandry
  - Human Cardiac RNA
  - Culturing of HL-1 Cells
- METHOD DETAILS
  - Permanent Left Anterior Descending (LAD) Coronary Artery Occlusion
  - Experimental Cardiomyopathy
  - Transverse Aortic Constriction (TAC) Surgery
  - Ultrasound Echocardiography
  - Treatment with GIPR agonists
  - Isolated Working Heart Perfusions and Assessment of Energy Metabolism
  - Histology and Assessment of Left Ventricle (LV) Infarct Scar Formation
  - Triacylglycerol (TAG) Determination
  - Isolation of Adult Cardiomyocyte and Non-Cardiomyocyte Fractions
  - Culturing of HEK293 Cells and Transient Transfection for Determining GIPR Antibody Specificity
  - Detection of Full Length Mouse *Gipr* mRNA
  - Detection of *GIPR* mRNA Expression in Human Heart
  - *In Situ* Hybridization
  - Cyclic AMP (cAMP) Assay
  - Real Time Quantitative PCR
  - Islet Isolation, Perifusion and Analysis of GIP(3-30)
  - Immunoblot Analysis
- QUANTIFICATION AND STATISTICAL ANALYSIS
  - Statistical Analysis

## SUPPLEMENTAL INFORMATION

Supplemental Information includes three figures and two tables and can be found with this article online at https://doi.org/10.1016/j.cmet.2017.11.003.

## ACKNOWLEDGMENTS

J.R.U. was supported by fellowships from the Canadian Institutes of Health Research (CIHR) and the Alberta Innovates-Health Solutions. J.E.C. has received fellowships from the Banting and Best Diabetes Centre (BBDC) and the CIHR. B.A.M. and H.E.B. received fellowships from the BBDC. H.E.B. received fellowship support from the Canadian Diabetes Association (CDA). S.A. has received a studentship from the BBDC. M.K. has received a fellowship from the CDA. E.E.M. has received fellowships from the CDA and the CIHR. D.J.D. has received funding from: the Heart and Stroke Foundation of Ontario G-14-0005953, CIHR grants 82700 and 154321, partial operating grant support from Merck for studies of cardiac GIP action, a Novo Nordisk postdoctoral training program grant, the Canada Research Chair in Regulatory Peptides, and a Banting and Best Diabetes Centre Novo Nordisk Chair in Incretin Biology. HL-1 cells were a generous gift from Dr. William Claycomb. Human heart tissue was provided via Dr. Kenneth B. Margulies at the University of Pennsylvania in Philadelphia, PA. We thank Chris Newgard and Olga Ilkayeva for helpful discussions surrounding analysis of cardiac metabolomics.

J.R.U. has received a speaker's honorarium for symposia sponsored by Novo Nordisk. E.M. and J.C. have received a speaker's honorarium for symposia sponsored by Merck. Y.S. reports consulting or speaking fees from Novo Nordisk, MSD, Takeda Pharmaceuticals, Sanofi, Taisho Toyama Pharmaceuticals, Eli Lilly and Company, Mitsubishi Tanabe Pharma, Ono Pharmaceutical, Kowa, Astellas Pharma, and Boehringer Ingelheim.

D.J.D. has served as an advisor or consultant to Arisaph Pharmaceuticals, Intarcia, Merck Research Laboratories, Novo Nordisk, and Pfizer Inc.

## AUTHOR CONTRIBUTIONS

Conceptualization, J.R.U. and D.J.D.; Investigation, J.R.U., J.E.C., E.E.M., L.L.B, H.E.B., B.A.M., K.G., M.C., B.Y., X.C., S.A., M.K., and M.G.K.; Formal Analysis & Visualization, J.R.U.; Writing – Original Draft, J.R.U. and D.J.D.; Writing – Review & Editing, J.R.U., J.E.C., E.E.M., Y.S., L.L.B., B.Y., J.S., and D.J.D.; Funding Acquisition and Project Administration, D.J.D.; Resources, Y.S., J.S., and D.J.D.; Supervision, D.J.D. D.J.D. takes full responsibility for the data within this paper.

Received: February 2, 2017
Revised: October 15, 2017
Accepted: November 15, 2017
Published: December 21, 2017

## REFERENCES

Ali, S., Ussher, J.R., Baggio, L.L., Kabir, M.G., Charron, M.J., Ilkayeva, O., Newgard, C.B., and Drucker, D.J. (2014). Cardiomyocyte glucagon receptor signaling modulates outcomes in mice with experimental myocardial infarction. Mol. Metab. *4*, 132–143.

Asmar, M., Asmar, A., Simonsen, L., Gasbjerg, L.S., Sparre-Ulrich, A.H., Rosenkilde, M.M., Hartmann, B., Dela, F., Holst, J.J., and Bülow, J. (2017). The gluco- and liporegulatory and vasodilatory effects of glucose-dependent insulinotropic polypeptide (GIP) are abolished by an antagonist of the human GIP receptor. Diabetes *66*, 2363–2371.

Bates, H.E., Campbell, J.E., Ussher, J.R., Baggio, L.L., Maida, A., Seino, Y., and Drucker, D.J. (2012). Gipr is essential for adrenocortical steroidogenesis; however, corticosterone deficiency does not mediate the favorable metabolic phenotype of Gipr(-/-) mice. Diabetes *61*, 40–48.

Berglund, L.M., Lyssenko, V., Ladenvall, C., Kotova, O., Edsfeldt, A., Pilgaard, K., Alkayyali, S., Brøns, C., Forsblom, C., Jonsson, A., et al. (2016). Glucose-dependent insulinotropic polypeptide stimulates osteopontin expression in the vasculature via endothelin-1 and CREB. Diabetes *65*, 239–254.

Campbell, J.E., and Drucker, D.J. (2013). Pharmacology, physiology, and mechanisms of incretin hormone action. Cell Metab. *17*, 819–837.

Campbell, J.E., Ussher, J.R., Mulvihill, E.E., Kolic, J., Baggio, L.L., Cao, X., Liu, Y., Lamont, B.J., Morii, T., Streutker, C.J., et al. (2016). TCF1 links GIPR signaling to the control of beta cell function and survival. Nat. Med. *22*, 84–90.

Claycomb, W.C., Lanson, N.A., Jr., Stallworth, B.S., Egeland, D.B., Delcarpio, J.B., Bahinski, A., and Izzo, N.J., Jr. (1998). HL-1 cells: a cardiac muscle cell line that contracts and retains phenotypic characteristics of the adult cardiomyocyte. Proc. Natl. Acad. Sci. USA *95*, 2979–2984.

Drucker, D.J. (2016). The Cardiovascular biology of glucagon-like peptide-1. Cell Metab. *24*, 15–30.

Duan, R.D., and Erlanson-Albertsson, C. (1992). Gastric inhibitory polypeptide stimulates pancreatic lipase and colipase synthesis in rats. Am. J. Physiol. *262*, G779–G784.

Eckel, R.H., Fujimoto, W.Y., and Brunzell, J.D. (1979). Gastric inhibitory polypeptide enhanced lipoprotein lipase activity in cultured preadipocytes. Diabetes *28*, 1141–1142.

Finan, B., Ma, T., Ottaway, N., Müller, T.D., Habegger, K.M., Heppner, K.M., Kirchner, H., Holland, J., Hembree, J., Raver, C., et al. (2013). Unimolecular dual incretins maximize metabolic benefits in rodents, monkeys, and humans. Sci. Transl. Med. *5*, 209ra151.

Finan, B., Yang, B., Ottaway, N., Smiley, D.L., Ma, T., Clemmensen, C., Chabenne, J., Zhang, L., Habegger, K.M., Fischer, K., et al. (2015). A rationally designed monomeric peptide triagonist corrects obesity and diabetes in rodents. Nat. Med. *21*, 27–36.

Finan, B., Müller, T.D., Clemmensen, C., Perez-Tilve, D., DiMarchi, R.D., and Tschöp, M.H. (2016). Reappraisal of GIP Pharmacology for Metabolic Diseases. Trends Mol. Med. *22*, 359–376.

Frias, J.P., Bastyr, E.J., 3rd, Vignati, L., Tschop, M.H., Schmitt, C., Owen, K., Christensen, R.H., and DiMarchi, R.D. (2017). The sustained effects of a dual GIP/GLP-1 receptor agonist, NNC0090-2746, in patients with type 2 diabetes. Cell Metab. *26*, 343–352.e2.

Gopal, K., Saleme, B., Al Batran, R., Aburasayn, H., Eshreif, A., Ho, K.L., Ma, W.K., Almutairi, M., Eaton, F., Gandhi, M., et al. (2017). FoxO1 regulates myocardial glucose oxidation rates via transcriptional control of pyruvate dehydrogenase kinase 4 expression. Am. J. Physiol. Heart Circ. Physiol. *313*, H479–H490.

Hansotia, T., Baggio, L.L., Delmeire, D., Hinke, S.A., Yamada, Y., Tsukiyama, K., Seino, Y., Holst, J.J., Schuit, F., and Drucker, D.J. (2004). Double incretin receptor knockout (DIRKO) mice reveal an essential role for the enteroinsular axis in transducing the glucoregulatory actions of DPP-IV inhibitors. Diabetes *53*, 1326–1335.

Harada, N., Yamada, Y., Tsukiyama, K., Yamada, C., Nakamura, Y., Mukai, E., Hamasaki, A., Liu, X., Toyoda, K., Seino, Y., and Inagaki, N. (2008). A novel GIP receptor splice variant influences GIP sensitivity of pancreatic beta-cells in obese mice. Am. J. Physiol. Endocrinol. Metab. *294*, E61–E68.

Højberg, P.V., Vilsbøll, T., Rabøl, R., Knop, F.K., Bache, M., Krarup, T., Holst, J.J., and Madsbad, S. (2009). Four weeks of near-normalisation of blood glucose improves the insulin response to glucagon-like peptide-1 and glucose-dependent insulinotropic polypeptide in patients with type 2 diabetes. Diabetologia *52*, 199–207.

Jones, I.R., Owens, D.R., Luzio, S.D., and Hayes, T.M. (1989). Obesity is associated with increased post-prandial GIP levels which are not reduced by dietary restriction and weight loss. Diabete Metab. *15*, 11–22.

Kaul, S. (2017). Mitigating cardiovascular risk in type 2 diabetes with antidiabetes drugs: a review of principal cardiovascular outcome results of EMPA-REG OUTCOME, LEADER, and SUSTAIN-6 trials. Diabetes Care *40*, 821–831.

Kim, M., Platt, M.J., Shibasaki, T., Quaggin, S.E., Backx, P.H., Seino, S., Simpson, J.A., and Drucker, D.J. (2013). GLP-1 receptor activation and Epac2 link atrial natriuretic peptide secretion to control of blood pressure. Nat. Med. *19*, 567–575.

Koitabashi, N., Bedja, D., Zaiman, A.L., Pinto, Y.M., Zhang, M., Gabrielson, K.L., Takimoto, E., and Kass, D.A. (2009). Avoidance of transient cardiomyopathy in cardiomyocyte-targeted tamoxifen-induced MerCreMer gene deletion models. Circ. Res. *105*, 12–15.

Livak, K.J., and Schmittgen, T.D. (2001). Analysis of relative gene expression data using real-time quantitative PCR and the 2(-Delta Delta C(T)) Method. Methods *25*, 402–408.

Lopaschuk, G.D., Ussher, J.R., Folmes, C.D., Jaswal, J.S., and Stanley, W.C. (2010). Myocardial fatty acid metabolism in health and disease. Physiol. Rev. *90*, 207–258.

Miyawaki, K., Yamada, Y., Yano, H., Niwa, H., Ban, N., Ihara, Y., Kubota, A., Fujimoto, S., Kajikawa, M., Kuroe, A., et al. (1999). Glucose intolerance caused by a defect in the entero-insular axis: a study in gastric inhibitory polypeptide receptor knockout mice. Proc. Natl. Acad. Sci. USA *96*, 14843–14847.

Mulvihill, E.E., Varin, E.M., Ussher, J.R., Campbell, J.E., Bang, K.W., Abdullah, T., Baggio, L.L., and Drucker, D.J. (2016). Inhibition of dipeptidyl peptidase-4 impairs ventricular function and promotes cardiac fibrosis in high fat-fed diabetic mice. Diabetes *65*, 742–754.

Nasteska, D., Harada, N., Suzuki, K., Yamane, S., Hamasaki, A., Joo, E., Iwasaki, K., Shibue, K., Harada, T., and Inagaki, N. (2014). Chronic reduction of GIP secretion alleviates obesity and insulin resistance under high-fat diet conditions. Diabetes *63*, 2332–2343.

Neilan, T.G., Blake, S.L., Ichinose, F., Raher, M.J., Buys, E.S., Jassal, D.S., Furutani, E., Perez-Sanz, T.M., Graveline, A., Janssens, S.P., et al. (2007). Disruption of nitric oxide synthase 3 protects against the cardiac injury, dysfunction, and mortality induced by doxorubicin. Circulation *116*, 506–514.

Noyan-Ashraf, M.H., Momen, M.A., Ban, K., Sadi, A.M., Zhou, Y.Q., Riazi, A.M., Baggio, L.L., Henkelman, R.M., Husain, M., and Drucker, D.J. (2009). GLP-1R agonist liraglutide activates cytoprotective pathways and improves outcomes after experimental myocardial infarction in mice. Diabetes *58*, 975–983.

O'Connell, T.D., Rodrigo, M.C., and Simpson, P.C. (2007). Isolation and culture of adult mouse cardiac myocytes. Methods Mol. Biol. *357*, 271–296.

Pyke, C., Heller, R.S., Kirk, R.K., Ørskov, C., Reedtz-Runge, S., Kaastrup, P., Hvelplund, A., Bardram, L., Calatayud, D., and Knudsen, L.B. (2014). GLP-1 receptor localization in monkey and human tissue: novel distribution revealed with extensively validated monoclonal antibody. Endocrinology *155*, 1280–1290.

Quaife-Ryan, G.A., Sim, C.B., Ziemann, M., Kaspi, A., Rafehi, H., Ramialison, M., El-Osta, A., Hudson, J.E., and Porrello, E.R. (2017). Multicellular transcriptional analysis of mammalian heart regeneration. Circulation *136*, 1123–1139.

Sauvé, M., Ban, K., Momen, M.A., Zhou, Y.-Q., Henkelman, R.M., Husain, M., and Drucker, D.J. (2010). Genetic deletion or pharmacological inhibition of dipeptidyl peptidase-4 improves cardiovascular outcomes after myocardial infarction in mice. Diabetes *59*, 1063–1073.

Sparre-Ulrich, A.H., Gabe, M.N., Gasbjerg, L.S., Christiansen, C.B., Svendsen, B., Hartmann, B., Holst, J.J., and Rosenkilde, M.M. (2017). GIP(3-30)NH2 is a potent competitive antagonist of the GIP receptor and effectively inhibits GIP-mediated insulin, glucagon, and somatostatin release. Biochem. Pharmacol. *131*, 78–88.

Timper, K., Grisouard, J., Sauter, N.S., Herzog-Radimerski, T., Dembinski, K., Peterli, R., Frey, D.M., Zulewski, H., Keller, U., Müller, B., and Christ-Crain, M. (2013). Glucose-dependent insulinotropic polypeptide induces cytokine expression, lipolysis, and insulin resistance in human adipocytes. Am. J. Physiol. Endocrinol. Metab. *304*, E1–E13.

Tschöp, M.H., Finan, B., Clemmensen, C., Gelfanov, V., Perez-Tilve, D., Müller, T.D., and DiMarchi, R.D. (2016). Unimolecular polypharmacy for treatment of diabetes and obesity. Cell Metab. *24*, 51–62.

Ueno, M., Suzuki, J., Zenimaru, Y., Takahashi, S., Koizumi, T., Noriki, S., Yamaguchi, O., Otsu, K., Shen, W.J., Kraemer, F.B., and Miyamori, I. (2008). Cardiac overexpression of hormone-sensitive lipase inhibits myocardial steatosis and fibrosis in streptozotocin diabetic mice. Am. J. Physiol. Endocrinol. Metab. *294*, E1109–E1118.

Ussher, J.R., Koves, T.R., Jaswal, J.S., Zhang, L., Ilkayeva, O., Dyck, J.R., Muoio, D.M., and Lopaschuk, G.D. (2009). Insulin-stimulated cardiac glucose oxidation is increased in high-fat diet-induced obese mice lacking malonyl CoA decarboxylase. Diabetes *58*, 1766–1775.

Ussher, J.R., Folmes, C.D., Keung, W., Fillmore, N., Jaswal, J.S., Cadete, V.J., Beker, D.L., Lam, V.H., Zhang, L., and Lopaschuk, G.D. (2012). Inhibition of serine palmitoyl transferase I reduces cardiac ceramide levels and increases glycolysis rates following diet-induced insulin resistance. PLoS One *7*, e37703.

Ussher, J.R., Baggio, L.L., Campbell, J.E., Mulvihill, E.E., Kim, M., Kabir, M.G., Cao, X., Baranek, B.M., Stoffers, D.A., Seeley, R.J., and Drucker, D.J. (2014). Inactivation of the cardiomyocyte glucagon-like peptide-1 receptor (GLP-1R) unmasks cardiomyocyte-independent GLP-1R-mediated cardioprotection. Mol. Metab. *3*, 507–517.

Wisneski, J.A., Stanley, W.C., Neese, R.A., and Gertz, E.W. (1990). Effects of acute hyperglycemia on myocardial glycolytic activity in humans. J. Clin. Invest. *85*, 1648–1656.

## STAR★METHODS

### KEY RESOURCES TABLE

| REAGENT or RESOURCE | SOURCE | IDENTIFIER |
|---|---|---|
| Antibodies | | |
| Anti-Akt | Cell Signaling | Cat#9272 |
| Anti-Phospho-Akt (Ser473) | Cell Signaling | Cat#9271 |
| Anti-GSK3alpha/beta | Cell Signaling | Cat#9315 |
| Anti-Phospho-GSK3beta (Ser9) | Cell Signaling | Cat#8566 |
| Anti-AMPKalpha | Cell Signaling | Cat#2532 |
| Anti-Phospho-AMPKalpha (Thr172) | Cell Signaling | Cat#2535 |
| Anti-ATGL | Cell Signaling | Cat#2439 |
| Anti-Phospho-HSL (Ser660) | Cell Signaling | Cat#4126 |
| Anti-Phospho-HSL (Ser563) | Cell Signaling | Cat#4139 |
| Anti-HSL | Cell Signaling | Cat#4107 |
| Anti-Phospho-ERK1/2 (Thr202/Tyr204) | Cell Signaling | Cat#4377 |
| Anti-ERK1/2 | Cell Signaling | Cat#4695 |
| Anti-Phospho-VASP (Ser239) | Cell Signaling | Cat#3114 |
| Anti-VASP | Cell Signaling | Cat#3112 |
| Anti-ACE2 | Cell Signaling | Cat#4355 |
| Anti-SPARC | Cell Signaling | Cat#5420 |
| Anti-Caveolin-1 | Cell Signaling | Cat#3238 |
| Anti-Mif-1 | Abcam | Cat#Ab7207 |
| Anti-hsp90 | BD Biosciences | Cat#610418 |
| Anti-GIPR | ABclone | Cat#A9816 |
| Anti-GIPR | Novus | Cat#NLS1251 |
| Anti-GIPR | Abcam | Cat#AB198694 |
| Anti-FLAG | Cell Signaling | Cat#2368 |
| Chemicals, Peptides, and Recombinant Proteins | | |
| D-Ala2-GIP | CHI Scientific | Custom synthesis |
| GIP(3-30) | CHI Scientific | Custom synthesis |
| Insulin (Humulin) | Eli Lilly and Co.Bio | Cat#VL7510 |
| ZD 7114 | Sigma | Cat#Z4902 |
| H89 | Sigma | Cat#B1427 |
| Rp-cAMP | Sigma | Cat#A165 |
| Forskolin | Sigma | Cat#F3917 |
| ESCA-AM | Fisher Scientific | Cat#48-531-00U |
| 8-Br-cGMP | Sigma | Cat#B1381 |
| Rp-8-Br-cGMPS | Sigma | Cat#SML1614 |
| Doxorubicin | Sigma | Cat#D1515 |
| U0126 | Calbiochem | Cat#662005 |
| SB203580 | Calbiochem | Cat#559389 |
| Mm-Gipr-01 | Advanced Cell Diagnostics | Cat#455781 |
| Mm-Gipr-02 | Advanced Cell Diagnostics | Cat#455791 |
| Collagenase Type II | Worthington | Cat#LS004176 |
| Critical Commercial Assays | | |
| Ultrasensitive Mouse Insulin ELISA | ALPCO | Cat#80-INSMSU-E01 |
| Triglyceride Assay Kit | Roche | Cat#05171407190 |

(*Continued on next page*)

| Continued | | |
|---|---|---|
| REAGENT or RESOURCE | SOURCE | IDENTIFIER |
| cAMP Assay Kit | Biomedical Technologies Inc. | Cat#BT-300 |
| RNAscope 2.5 HD Reagent Kit-Red | Advanced Cell Diagnostics | Cat#322350 |
| Experimental Models: Cell Lines | | |
| HL-1 Cells | Live cells provided directly from Dr. William Claycomb's laboratory | N/A |
| HEK293 Cells | ATCC | Cat#CRL-1573 |
| Experimental Models: Organisms/Strains | | |
| C57BL/6J mice | In-house colony at the Toronto Centre for Phenogenomics | N/A |
| Floxed Gipr mice | Mice generated by Ingenious Targeting | N/A |
| MerCreMer mice | Jackson Laboratory | Stock#005657 |
| MIP-Cre mice | Jackson Laboratory | Stock#024709 |
| $Gipr^{-/-}$ mice | Mice provided via Dr. Yutaka Seino | N/A |
| alphaMHC-Lipe mice | Mice provided via Dr. Jinya Suzuki | N/A |
| Oligonucleotides | | |
| Mouse Gipr 5′ (CTGCTTCTGCTGCTGTGGT) | ACGT Corporation | Custom synthesis |
| Mouse Gipr 3′ (CACATGCAGCATCCCAGA) | ACGT Corporation | Custom synthesis |
| Mouse Gipr Internal Probe (GTCTGCAGGCTTTGTCTTCC) | ACGT Corporation | Custom synthesis |
| HSL siRNA | Santa Cruz | Cat#sc-77404 |
| Recombinant DNA | | |
| pFLAG-CMV-5b vector | Sigma | Cat#E7648 |
| Other | | |
| [U-14C]glucose | Perkin Elmer | Cat#NEC042A001MC |
| [9,10-3H]palmitate | Perkin Elmer | Cat#NET043005MC |

## CONTACT FOR REAGENT AND RESOURCE SHARING

Further information and requests for resources and reagents should be directed to the Lead Contact for this manuscript, Daniel Drucker (drucker@lunenfeld.ca).

## EXPERIMENTAL MODEL AND SUBJECT DETAILS

### Animal Husbandry

All procedures were conducted according to protocols and guidelines approved by the Toronto Centre for Phenogenomics (TCP) Animal Care Committee. Experiments were conducted in male mice acclimatized to handling and housed under a 12-h light/dark cycle with free access to standard rodent diet (2018, 18% kcal from fat; Harlan Teklad, Mississauga, ON, Canada) and water, unless otherwise noted. C57BL/6J mice were obtained from an internal TCP colony. The generation and characterization of $Gipr^{-/-}$ mice has been described previously (Miyawaki et al., 1999). To generate $Gipr^{-/-}$ mice with cardiac-specific overexpression of HSL (*Lipe*) ($Gipr^{-/-}$:MHC-*Lipe* mice), we crossed mice overexpressing *Lipe* in the heart (Ueno et al., 2008) with $Gipr^{-/-}$ mice. To generate $Gipr^{CM-/-}$ mice, MerCreMer transgenic mice expressing tamoxifen-inducible Cre were bred with floxed *Gipr* mice (Campbell et al., 2016). Cre-induced inactivation of the *Gipr* gene was carried out via 6 intraperitoneal (*i.p.*) injections of tamoxifen (50 mg/kg) over 8 days (Ussher et al., 2014). To minimize effects from transient, reversible cardiomyopathy (Koitabashi et al., 2009), mice were allowed 5 weeks to recover before experimentation. All mice were 10-12 weeks of age prior to experimentation, and all mice were housed at room temperature. Expanded information on animal characteristics is provided in the Method Details below.

### Human Cardiac RNA

RNA was prepared from all 4 chambers of 15 different human heart samples obtained from the University of Pennsylvania Heart BioBank, via Dr. Ken Margulies. Tissues from failing human hearts were obtained from male patients receiving heart transplantation at the University of Pennsylvania. The use of human heart tissue for research was approved by the University of Pennsylvania's Institutional Review Board. Non-failing heart tissue was obtained from deceased organ donors through the Gift-of-Life donor program in Philadelphia. Prospective informed consent for research use of heart tissue was obtained from all transplant recipients and from the appropriate next of kin for the organ donors. All human tissues received *in situ* high-potassium cardioplegia at the time of tissue

procurement and were kept on wet ice for less than four hours before fixation in freshly prepared paraformaldehyde. Further details on patient characteristics are described in Table S2.

### Culturing of HL-1 Cells

The HL-1 cell line was established from an AT-1 tumor excised from subcutaneous tissue from a female adult C57BL/6J mouse originating from the Jackson Laboratory (Claycomb et al., 1998). HL-1 cells were cultured in Claycomb media (Sigma) as previously described (Ali et al., 2014). Prior to all drug treatments, cells were serum starved in serum-free high glucose Dulbecco's Modified Eagle's Medium (DMEM, Sigma) containing 1% penicillin/streptomycin for 3 hr. To determine intracellular TAG content, cells were lipid loaded overnight with serum-free Claycomb media containing 0.4 mM oleic acid (Sigma) bound to 2% bovine serum albumin (BSA), followed by media change to serum-free Claycomb media without oleic acid and treatment with various drugs/peptides. All drugs and inhibitors including ZD 7114 were purchased from Sigma, whereas D-$Ala_2$ GIP was purchased from Chi Scientific.

## METHOD DETAILS

### Permanent Left Anterior Descending (LAD) Coronary Artery Occlusion

Experimental myocardial infarction (MI) was induced via permanent ligation of the left anterior descending (LAD) coronary artery in 10-12-week-old male *Gipr*$^{-/-}$ mice and their *Gipr*$^{+/+}$ littermates, 10-12-week-old male *Gipr*$^{-/-}$:MHC-*Lipe* mice, or 10-12-week-old male *Gipr*$^{CM-/-}$ mice and their αMHC-Cre littermates as previously described (Noyan-Ashraf et al., 2009). Sham-operated mice underwent the same procedure by moving the suture underneath the LAD coronary artery but without tying off the vessel. The surgeon was blinded to the genotypes of all mice for all surgeries. During post-operation recovery, mice were returned to their cages, which were placed on a heating pad for ~2 hr to assist mice in maintaining body temperature prior to animals being returned to their appropriate animal housing within the TCP. Cardiac examinations were performed on all deceased mice. The presence of a large amount of blood or clot around the heart and in the thoracic cavity, in addition to a perforation of the infarct or peri-infarct area was indicative of cardiac rupture.

### Experimental Cardiomyopathy

Experimental cardiomyopathy was induced via single *i.p.* injection of the anticancer anthracycline (drug class made from the bacteria *Streptomyces peucetius*) agent doxorubicin (20 mg/kg) in *Gipr*$^{-/-}$ mice and their *Gipr*$^{+/+}$ littermates as previously described (Neilan et al., 2007). Mice were followed for 10 days and hearts from surviving mice underwent histological assessment, or analysis of protein expression.

### Transverse Aortic Constriction (TAC) Surgery

In order to induce pressure-overload hypertrophy, an oblique 8-mm incision was made 2 mm away from the left sternal border and the transverse aortic arch was banded between the innominate artery and the left common carotide artery with a 28 gauge needle using a 7-0 silk suture in *Gipr*$^{-/-}$ mice and their *Gipr*$^{+/+}$ littermates as previously described (Mulvihill et al., 2016). Sham-operated mice underwent the same procedure by moving the suture behind the transverse aortic arch but without tying it off. The surgeon was blinded to the genotypes of all mice for all surgeries. During post-operation recovery, mice were returned to their cages, which were placed on a heating pad for ~2 hr to assist mice in maintaining body temperature prior to animals being returned to their appropriate animal housing within the TCP.

### Ultrasound Echocardiography

Transthoracic echocardiography ultrasound was performed in 3% isoflurane-anesthetized mice (30–40 MHz; Vevo770, VisualSonics,Toronto, Canada) that had their body temperature maintained and continually monitored/recorded on a heating device, for the assessment of LV function and LV wall structure pre-surgery and post-surgery (MI and TAC), as previously described (Mulvihill et al., 2016). The operator was blinded to the genotypes of all mice for these ultrasound experiments.

### Treatment with GIPR agonists

In subsets of experiments involving the assessment of systemic GIPR agonism of myocardial signaling, groups of mice were treated with D-$Ala_2$ GIP (24 nmol/kg BW) immediately after an overnight fast and hearts were extracted 1 hr post-treatment. To assess consequences of GIPR activation before induction of ischemia, D-$Ala_2$ GIP (24 nmol/kg BW) was administered twice daily for 1 week before experimental MI. All injections took place between 7:00 – 8:00 am and 4:00 – 5:00 pm.

### Isolated Working Heart Perfusions and Assessment of Energy Metabolism

Mice were anaesthetized with sodium pentobarbital (60 mg/kg IP), and the hearts were subsequently excised and immersed in ice-cold Krebs-Henseleit bicarbonate solution, following which the aorta was cannulated and equilibrated in the Langendorff mode. From here, the left atria was subsequently cannulated, allowing hearts to receive perfusate through the left atrium that enters the left ventricle and is subsequently ejected through the aorta during working mode perfusion as previously described (Gopal et al., 2017; Ussher et al., 2009). In brief, oxygenated Krebs-Henseleit solution consisting of 0.8 mM [9,10-$^{3}$H]palmitate bound to 3% fatty acid free bovine serum albumin and 5.5 mM [U-$^{14}$C]glucose was delivered to the left atrium at a preload pressure of 15 mmHg, while

perfusate was ejected from hearts into the aortic outflow line against a hydrostatic afterload pressure of 50 mmHg. Hearts were perfused aerobically for 80 min and glucose and palmitate oxidation were assessed as previously described (Gopal et al., 2017; Ussher et al., 2009). At the end of perfusion, hearts were immediately frozen in liquid $N_2$ with Wollenberger tongs, and stored at −80°C.

### Histology and Assessment of Left Ventricle (LV) Infarct Scar Formation

Animals were anesthetized using avertin (250 mg/kg *i.p.* injection). The chest was opened and an apical injection of 1 M KCl arrested the heart in diastole. Hearts were perfusion-fixed with 4% buffered formalin at physiological pressure, post-fixed in formalin, embedded in paraffin, sectioned at 6 μm, and stained with Masson's Trichrome or hematoxylin and eosin (H&E). Cardiac morphometry was performed with Aperio ImageScope Viewer software (Aperio Technologies) using digital planimetry to quantify the 2-dimensional area/region of infarcted scar from LV cross sections of high resolution digital photographs (Noyan-Ashraf et al., 2009; Sauvé et al., 2010). Infarcted/scarred LV area was calculated as a % of total LV area and the analysis was not blinded. Cardiac hypertrophy was quantified as the ventricular weight-to-body weight ratio.

### Triacylglycerol (TAG) Determination

TAGs were extracted from frozen ventricular tissue or cell pellets (20 – 30 mg) with a 2:1 chloroform-methanol solution and quantified with a commercially available enzymatic assay kit (Wako Pure Chemical Industries) as previously described (Ussher et al., 2009).

### Isolation of Adult Cardiomyocyte and Non-Cardiomyocyte Fractions

Cardiomyocyte and non-cardiomyocyte fractions were prepared from adult mouse ventricles as described (O'Connell et al., 2007) with the following modifications: 1) Ventricles were digested using 1.5 mg/ml collagenase II (Worthington Biochemicals, Lakewood, NJ; Cat# LS004176), and 2) Following sedimentation of isolated cardiomyocytes via centrifugation at 20 g for 3 min, the supernatant was collected and centrifuged at 300 g for 5 min to pellet non-cardiomyocytes.

### Culturing of HEK293 Cells and Transient Transfection for Determining GIPR Antibody Specificity

HEK293 cell lysates were prepared by homogenization in phosphate buffered saline supplemented with 1% Nonidet P-40, 0.5% sodium deoxycholate, 0.1% sodium dodecyl sulfate and protease inhibitor cocktail (Sigma-Aldrich, Oakville, Ontario, Canada). Lysates were cleared by centrifugation and then treated for 1 hr at 37 C with sample buffer containing β-mercaptoethanol. 40 μg of protein were resolved by discontinuous SDS-PAGE and then electrotransferred onto Amersham Protran nitrocellulose membrane (GE Healthcare Life Sciences, Mississauga ON Canada) using standard procedures. Blots were probed at room temperature with antibodies diluted in 5% skim milk in Tris buffered saline containing 0.2% Tween-20. Antigen-antibody complexes were visualized with a secondary antibody conjugated to horseradish peroxidase and an enhanced chemiluminescence kit (Perkin Elmer). Chemiluminescence detection was performed on a Kodak Imager. The following rabbit polyclonal antibodies to the GIP receptor were used, all at a dilution of 1:500: A9816 (ABclonal, Woburn MA), NLS1251 (Novus Biologicals, Oakville ON Canada), and ab198694 (Abcam, Cambridge, MA). The rabbit polyclonal anti-FLAG antibody (cat# 2368, 1:2500 dilution) was from Cell Signaling Technology (Whitby ON Canada). Transient transfection of HEK293 cells with the murine GIP receptor cloned into the pFLAG-CMV-5b vector (GipR-FLAG; Sigma, St. Louis, MO) (Harada et al., 2008) was done using Lipofectamine 2000 reagent (Invitrogen Life Technologies, Thermo Fisher Scientific) according to the manufacturer's protocol.

### Detection of Full Length Mouse *Gipr* mRNA

Total RNA was isolated using TRIzol reagent (Sigma). 2 μg total RNA was reversed transcribed at 50°C for 60 min using Superscript III reverse transcriptase and random hexamer primers (Sigma). The mouse GIPR was amplified by PCR using primer pairs 5′-CTG CTT CTG CTG CTG TGG T-3′ and 5′-CAC ATG CAG CAT CCC AGA-3′. Amplification of mouse GIPR cDNA resulted in generation of an approximately 1.5-kb product spanning bases 79–1486 of the GIPR open reading frame. After gel electrophoresis and transfer to nylon membranes, blots were hybridized with a $^{32}$P-labeled mouse (5′-GCTGTATCTGAGCATAGGCT-3′) GIPR oligonucleotide probe overnight. After washing, blots were exposed to a phosphorimaging cassette and visualized using a Storm 860 Phosphor Screen and analyzed with Quantity One imaging software (Bio-Rad).

### Detection of *GIPR* mRNA Expression in Human Heart

Human tissues from all 4 heart chambers (left atria, right atria, left ventricle, right ventricle) were pulverized in liquid nitrogen. Total RNA was extracted using Tri Reagent (Molecular Research Center Inc., Cincinnati, OH). cDNA was synthesized from 1 μg of DNase I-treated (Thermo-Fisher Scientific) total RNA using random hexamers and Superscript III (Thermo-Fisher Scientific). A 1.35 kb PCR product encompassing the majority of the human GIPR coding region was amplified from cDNA using the primer pairs 5′-TGA CTA CCT CTC CGA TCC TG-3′ and 5′-AGG GTC CCC GAG GAC AAG-3.' PCR products were separated on agarose gels, transferred to nylon membranes and hybridized with an internal human GIPR-specific $^{32}$P-labeled oligonucleotide probe (5′-CTC CTG TCC AAG CTG AGG AC-3′). Blots were exposed to a Storm 860 Phosphor Screen and visualized using Quantity One imaging software (Bio-Rad).

### *In Situ* Hybridization

For *in situ* hybridization, mouse hearts were formalin-fixed for 24 hr, embedded in paraffin, cut into 5 μm sections and mounted onto Superfrost Plus (Thermo-Fisher Scientific) glass slides. *In situ* hybridization for mouse *Gipr* was performed using the RNAscope 2.5 HD Detection Reagent kit (Advanced Cell Diagnostics Inc.) and mouse *Gipr* specific hybridization probes Mm-*Gipr*-01 and Mm-*Gipr*-02 (Cat# 455781 and 455791, respectively; Advanced Cell Diagnostics Inc.) according to the manufacturer's instructions. Slides were scanned at 40X and imaged using Aperio Image Scope v11.2.0.780 software (Leica Biosystems Imaging Inc.).

### Cyclic AMP (cAMP) Assay

cAMP levels were quantified in HL-1 cells cultured in 24-well plates and treated with various concentrations of [D-Ala$_2$]GIP using a radioimmunoassay kit as previously described (Bates et al., 2012). This kit utilizes a highly immunoreactive [$I^{125}$]S-cyclic AMP-tyrosyl methyl ester with specific primary antibodies conjugated to secondary antibodies, thereby minimizing non-specific binding and requiring only one incubation step.

### Real Time Quantitative PCR

First-strand cDNA was synthesized from total RNA of myocardial extracts using the SuperScript III synthesis system (Invitrogen, Carlsbad, CA). Real time PCR was carried out with the ABI Prism 7900 Sequence Detection System using TaqMan Gene Expression Assays (Applied Biosystems, Foster City, CA). Relative changes in mRNA transcript levels between experimental groups were quantified with the $2^{-\Delta\Delta Ct}$ method as previously described (Livak and Schmittgen, 2001), which assumes that the amplification efficiencies of the target and internal control genes are near identical. For our purposes cyclophilin was chosen as a house keeping internal control gene, as it was not affected by our experimental manipulations or by genotype in our studies.

### Islet Isolation, Perifusion and Analysis of GIP(3-30)

Islets were isolated from WT mice and perifused for 1 hr in Krebs-Ringer bicarbonate buffer with 2.7 mM glucose at a flow rate of 200 μL per min using the Biorep Perifusion system as previously described (Campbell et al., 2016). Insulin secretion was assessed in response to 10 mM glucose, 10 mM glucose plus 1 nM DA-GIP, and 10 mM glucose plus 1 nM DA-GIP and 1 uM GIP(3-30). Insulin values were determined by AlphaLISA assay (Perkin Elmer), following the manufactures instructions. The AUC was calculated for each condition, and the AUC for high-glucose alone was subtracted from the DA-GIP and DA-GIP+GIP(3-30) values. Data was then expressed as a percentage of DA-GIP to determine the percentage suppression by GIP(3-30).

### Immunoblot Analysis

Frozen ventricular tissue (20 mg) was homogenized and HL-1 cells lysed in buffer containing 50 mM Tris HCl (pH 8 at 4°C), 1 mM EDTA, 10% glycerol (wt/vol), 0.02% Brij-35 (wt/vol), 1 mM dithiothreitol, protease and phosphatase inhibitors (Sigma) as previously described (Ussher et al., 2012). Protein concentration of homogenates was determined via Bradford protein assay kit (Bio-Rad). Samples were resolved via 8% sodium dodecyl sulfate polyacrylamide gel electrophoresis (SDS-PAGE) and transferred onto a 0.20 μm nitrocellulose membrane. Membranes were blocked with 10% fat free milk for 2 hours and probed with either anti-HSL (Cell Signaling Technologies), anti-phosphoSerine-660 HSL (Cell Signaling Technologies), anti-phosphoSerine-563 HSL (Cell Signaling Technologies), anti-ERK (Cell Signaling Technologies), anti-phosphoThreonine-202/Tyrosine-204 ERK (Cell Signaling Technologies), anti-Akt (Cell Signaling Technologies), anti-phosphoSerine-473 Akt (Cell Signaling Technologies), anti-GSK3β (Cell Signaling Technologies), anti-phosphoSerine-9 GSK3β (Cell Signaling Technologies), anti-AMPK (Cell Signaling Technologies), anti-phosphoThreonine-172 AMPK (R&D Systems), anti-ATGL (Cell Signaling Technologies), anti-MIF-1 (Abcam), anti-SPARC4 (Cell Signaling Technologies), anti-caveolin-1 (Cell Signaling Technologies), anti-ACE II (Cell Signaling Technologies), and anti-hsp90 (BD Biosciences) antibodies in 5% fatty acid free bovine serum albumin. Immunoblots were visualized with the enhanced chemiluminescence western blot detection kit (Perkin Elmer) and quantified with Carestream Molecular Imaging Software (Kodak). A gel-documentation imager was used to visualize images detected by the secondary antibody bound to the primary antibody following emission of chemiluminescence (Perkin Elmer). As the molecular markers on the nitrocellulose membrane do not emit chemiluminescence, they do not appear on corresponding acquired image. Therefore, after image exposure, the nitrocellulose membrane itself was photographed, and the gel-doc-acquired image was subsequently overlayed on the nitrocellulose membrane image. The migration positions of the detected protein bands were then directly compared to the molecular markers from the protein ladder, to verify that individual protein bands corresponded to the expected molecular size based on the literature and the manufacturer's specifications (e.g., Phospho-Akt from Cell Signaling (9271) appearing at ~60 kDa). The molecular weights indicated for all proteins quantified by western blot analysis in our Figure Legends were determined in this specific manner.

## QUANTIFICATION AND STATISTICAL ANALYSIS

### Statistical Analysis

All values are presented as mean ± SE (*n* observations). The significance of differences was determined by a Kaplan Meier survival analysis, an unpaired, 2-tailed Student's t test, two-way analysis of variance (ANOVA), or a one-way ANOVA followed by a Bonferroni

post hoc analysis where appropriate. One-way ANOVA was performed when there were 3 or more experimental groups with one experimental outcome being measured (e.g., cAMP levels in response to various concentrations of [D-$Ala_2$]GIP). Conversely, two-way ANOVA was performed whenever an experimental outcome being measured was influenced by two experimental variables (e.g., cardiac TAG content in WT and *Gipr*$^{-/-}$ mice in response to either a 24 hr fast or a 24 hr fast-2 hr refeed). Differences were considered significant when $p < 0.05$. All statistical parameters can be found in the figure legends.

**Cell Metabolism, Volume *27***

## Supplemental Information

# Inactivation of the Glucose-Dependent Insulinotropic Polypeptide Receptor Improves Outcomes following Experimental Myocardial Infarction

**John R. Ussher, Jonathan E. Campbell, Erin E. Mulvihill, Laurie L. Baggio, Holly E. Bates, Brent A. McLean, Keshav Gopal, Megan Capozzi, Bernardo Yusta, Xiemin Cao, Safina Ali, Minsuk Kim, M. Golam Kabir, Yutaka Seino, Jinya Suzuki, and Daniel J. Drucker**

## Supplementary Figure 1

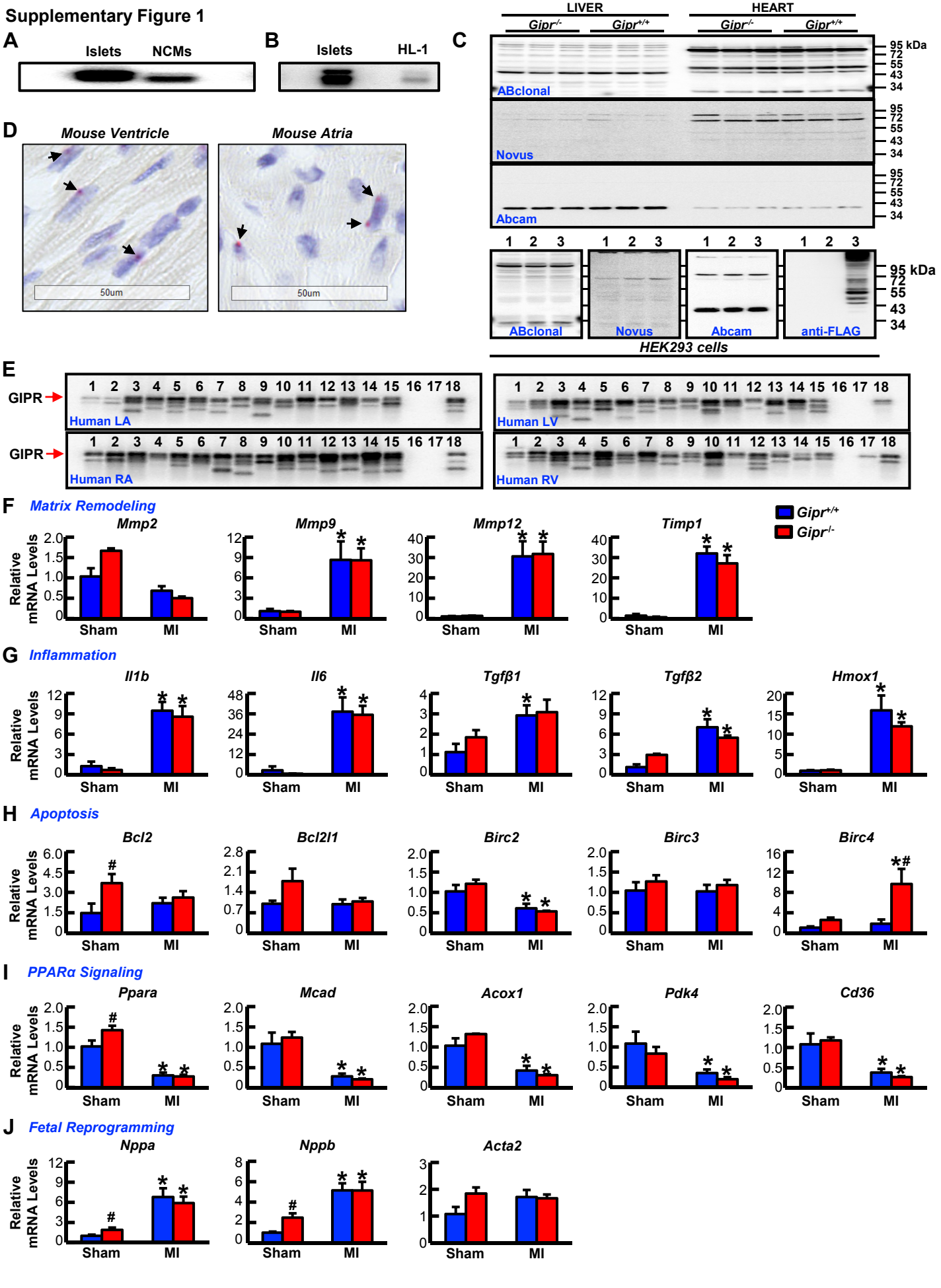

**Supplementary Figure 2**

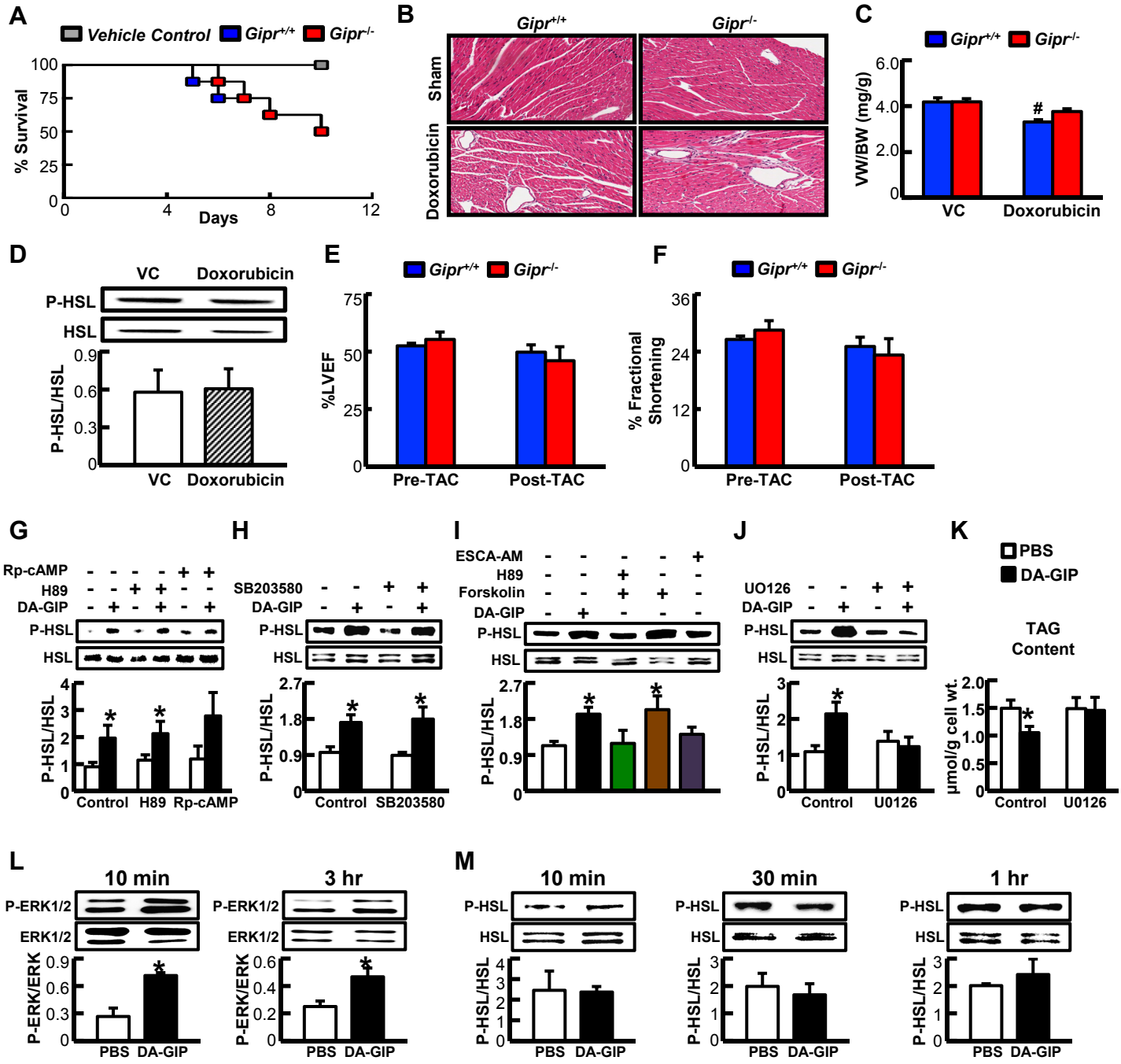

**Supplementary Figure 3**

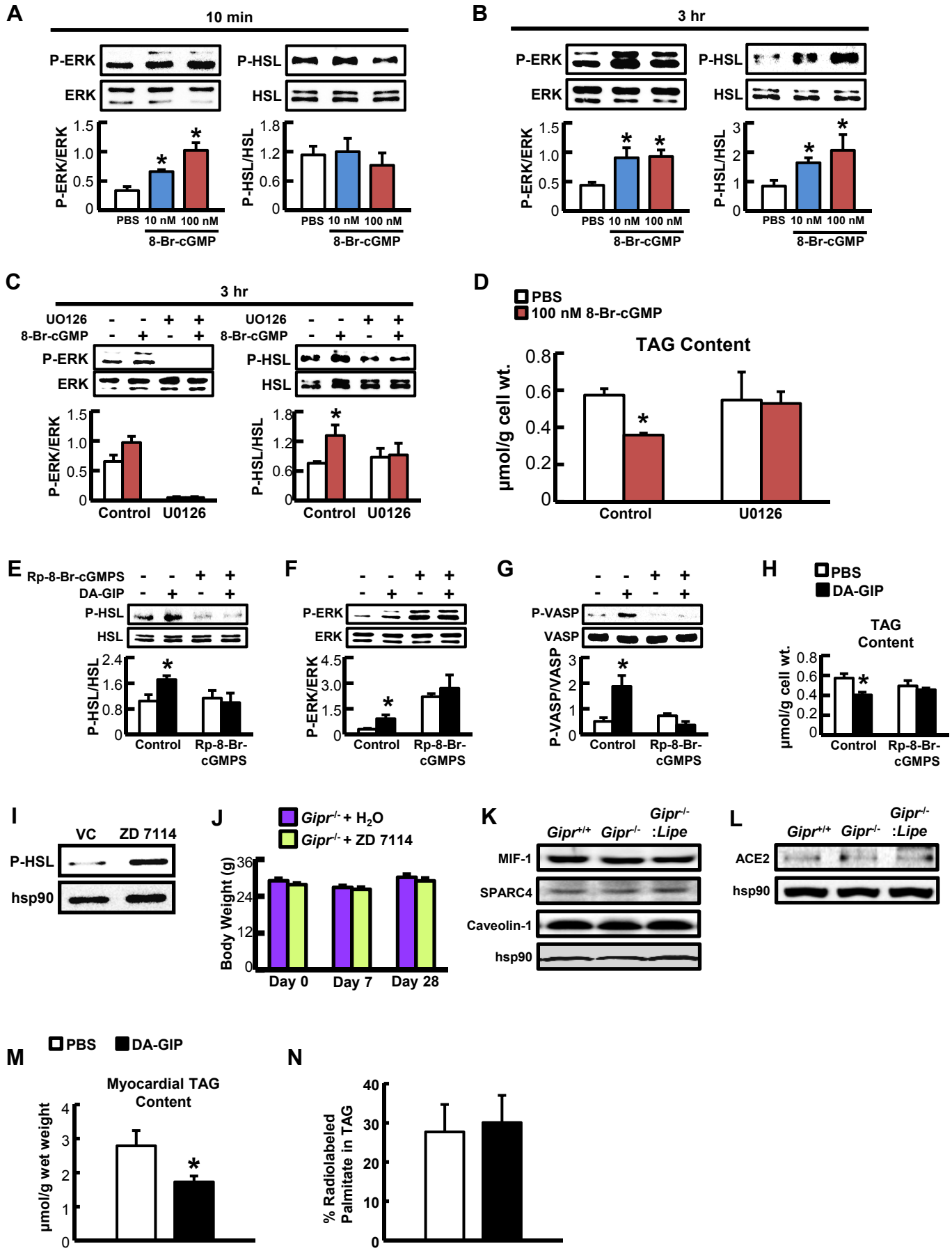

**SUPPLEMENTARY FIGURE LEGENDS**

**Figure S1. *Gipr* expression in cardiac myocytes and GIPR-dependent cardiac mRNA expression after myocardial infarction. Related to Figure 1 and Figure 2.** A: *Gipr* mRNA expression was detected in neonatal cardiac myocytes (NCMs) and B: HL-1 atrial cardiac myocytes by RT-PCR and blotting of PCR products followed by hybridization with an internal oligonucleotide probe specific to the mouse full length *Gipr* cDNA. C: Immunoblots characterizing the putative specificity of commercial GIPR antibodies using protein extracts from liver and heart of $Gipr^{+/+}$ and $Gipr^{-/-}$ mice. Bottom panel depicts Western blot analysis of HEK293 cells untransfected (lane 1), or transiently transfected with empty vector (lane 2) or the mouse *Gipr* cDNA cloned into pFLAG-CMV-5b (lane 3). Whole-cell extracts were prepared 36 hr after transfection and analyzed by immunoblotting with the specified GIPR commercial antibodies, or with a rabbit polyclonal anti-FLAG peptide tag antiserum. Molecular mass standards are indicated on the right. None of the 3 antibodies tested recognized the mouse GIPR, compared to the immunoreactive GIPR protein of ~ 51 kD detected with the Anti-FLAG antibody in lane 3. D: *In situ* hybridization demonstrating *Gipr*-positive (peri-nuclear red dots denoted by arrows) mouse ventricular and atrial cardiac myocytes. E: RT-PCR analysis of human heart RNA detects a *GIPR* mRNA (~1.35 kb), as well as several smaller transcripts, in all 4 chambers of the human heart, visualized by Southern blotting utilizing an internal oligonucleotide probe specific to the human full length *GIPR* cDNA. 1 – 15 = human heart samples, 16 = negative control ($H_2O$), 17 = human liver, 18 = human fat. See Supplementary Table 2 for description of the human heart samples. F: Levels of mRNA transcripts for the extracellular matrix remodeling factors, *Mmp2*, *Mmp9*, *Mmp12*, and *Timp1* from sham-treated and infarcted (MI; viable myocardium) $Gipr^{+/+}$ and $Gipr^{-/-}$ mouse hearts 48 hrs post-LAD coronary artery occlusion. G: Levels of mRNA transcripts for genes regulating inflammation, specifically *Il1b*, *Il6*, *Tgfb1*, *Tgfb2*, and *Hmox1* from sham-treated and infarcted (viable myocardium) $Gipr^{+/+}$ and $Gipr^{-/-}$ mouse hearts 48 hrs post-LAD coronary artery occlusion. H: Levels of mRNA transcripts for genes regulating apoptosis, *Bcl2*, *Bcl2l1*, *Birc2*, *Birc3*, and *Birc4* from sham-treated and infarcted (viable myocardium) $Gipr^{+/+}$ and $Gipr^{-/-}$ mouse hearts 48 hrs post-LAD

coronary artery occlusion. I: Levels of mRNA transcripts for *Ppara* and its downstream target genes, *Mcad*, *Acox1*, *Pdk4*, and *Cd36* from sham-treated and infarcted (viable myocardium) *Gipr*$^{+/+}$ and *Gipr*$^{-/-}$ mouse hearts 48 hrs post-LAD coronary artery occlusion. J: Levels of mRNA transcripts for genes involved in fetal reprogramming of the failing heart, *Nppa*, *Nppb*, and *Acta2* from sham-treated and infarcted (viable myocardium) *Gipr*$^{+/+}$ and *Gipr*$^{-/-}$ mouse hearts 48 hrs post-LAD coronary artery occlusion. Values represent mean ± SE (n = 3-5). Differences were determined using a 2-way ANOVA followed by a Bonferroni post-hoc analysis. **P*<0.05, significantly different from sham counterpart; $^{\#}$*P*<0.05, significantly different from *Gipr*$^{+/+}$ counterpart.

**Figure S2. *Gipr*$^{-/-}$ mice and experimental heart failure, and GIPR-mediated control of HSL phosphorylation in vitro. Related to Figures 1 – 3**

A: Survival in *Gipr*$^{+/+}$ and *Gipr*$^{-/-}$ mice treated with a single injection of vehicle alone or doxorubicin (20 mg/kg, *i.p.*). B: H&E stained ventricular cross sections from *Gipr*$^{+/+}$ and *Gipr*$^{-/-}$ mice at 10 days post-doxorubicin or vehicle (Sham). C: Ventricular weight/body weight (VW/BW) ratios in *Gipr*$^{+/+}$ and *Gipr*$^{-/-}$ mice at 10 days post-doxorubicin or vehicle control (VC). D: HSL serine 660 phosphorylation (81 – 83 kDa) in hearts from wild-type mice at 4 days post-treatment with either vehicle control (VC) or doxorubicin. E: % left ventricular ejection fraction (LVEF) and F: % fractional shortening in *Gipr*$^{+/+}$ and *Gipr*$^{-/-}$ mice pre-transverse aortic constriction (TAC) and at 4 weeks post-TAC (n = 6). G: HSL serine 660 phosphorylation (81 – 83 kDa) in HL-1 cells treated with either 15 μM H89 or 20 μM Rp-cAMP prior to treatment with 100 nM [D-Ala$_2$]GIP (DA-GIP) for 3 hrs (n = 3). H: HSL serine 660 phosphorylation (81 – 83 kDa) in HL-1 cells treated with 10 μM SB203580 prior to treatment with 100 nM DA-GIP for 3 hrs (n = 3). I: HSL serine 660 phosphorylation (81 – 83 kDa) in HL-1 cells treated with either 100 nM DA-GIP, 50 μM forskolin, or 10 μM 8-pCPT-2-O-Me-cAMP-AM (ESCA-AM) for 3 hrs (n = 3). J: HSL serine 660 phosphorylation (81 – 83 kDa) in HL-1 cells treated with 10 μM U0126 prior to treatment with 100 nM DA-GIP for 3 hrs (n = 3). K: Intracellular triacylglycerol (TAG) content in HL-1 cells lipid-loaded with 0.4 mM oleic acid bound to 2% BSA for 16 hrs and treated with 10 μM U0126 prior to treatment with 100 nM DA-

GIP for 4 hrs (n = 5-6). L: ERK (extracellular signal–regulated kinase) threonine 202/tyrosine 204 phosphorylation (42 – 44 kDa) in HL-1 cells treated with 100 nM DA-GIP for either 10 min or 3 hr (n = 3-5). M: HSL serine 660 phosphorylation (81 – 83 kDa) in HL-1 cells treated with 100 nM DA-GIP for 10 min , 30 min, or 1 hr. Values represent mean ± SE. Differences were determined using either an unpaired Student's two-tailed t-test, or a 1-way or 2-way ANOVA followed by a Bonferroni post-hoc analysis. $^{\#}P<0.05$, significantly different from VC-treated counterpart; $*P<0.05$, significantly different from PBS-treated counterpart.

**Figure S3. GIPR-mediated control of HSL phosphorylation, and genetic or pharmacological manipulation of HSL in *Gipr*$^{-/-}$ mice. Related to Figure 2 and Figure 3**

ERK threonine 202/tyrosine 204 phosphorylation (42 – 44 kDa) in HL-1 cells treated with 10 or 100 nM 8-Br-cGMP (8-Bromoguanosine 3′ ,5′ -cyclic monophosphate) for either A: 10 min or B: 3 hr (n = 4). C: ERK threonine 202/tyrosine 204 phosphorylation (42 – 44 kDa) and HSL serine 660 phosphorylation (81 – 83 kDa) in HL-1 cells treated with 10 μM U0126 prior to treatment with 100 nM 8-Br-cGMP for 3 hrs (n = 4-6). D: Intracellular triacylglycerol (TAG) content in HL-1 cells treated with 10 μM U0126 prior to treatment with 100 nM 8-Br-cGMP for 4 hrs (n = 3). E: HSL serine 660 phosphorylation (81 – 83 kDa) in HL-1 cells treated with 25 μM Rp-8-Br-cGMPS (Rp-8-Bromoguanosine-3,5-cyclic monophosphorothioate sodium salt) prior to treatment with 100 nM [D-Ala$_2$]GIP (DA-GIP) (n = 4). F: ERK threonine 202/tyrosine 204 phosphorylation (42 – 44 kDa) and G: VASP serine 239 phosphorylation (50 kDa) in HL-1 cells treated with 25 μM Rp-8-Br-cGMPS prior to treatment with 100 nM DA-GIP for 3 hrs (n = 4). H: Intracellular TAG content in HL-1 cells lipid-loaded with 0.4 mM oleic acid bound to 2% BSA for 16 hrs and treated with 25 μM Rp-8-Br-cGMPS prior to treatment with 100 nM DA-GIP for 4 hrs (n = 3). I: Myocardial HSL serine 660 phosphorylation (81 – 83 kDa) in C57BL/6J mice treated with either vehicle control (VC, $H_2O$) or 10 mg/kg ZD 7114 for 6 hrs after an overnight fast. J: Initial body weight and body weights 7 and 28 days following twice daily injection of either VC or ZD 7114 (10 mg/kg) in *Gipr*$^{-/-}$ mice (n = 8-10). K/L: MIF-1 (13 kDa) protein expression, SPARC4 (42

kDa) protein expression, Caveolin-1 (24 kDa) protein expression, and ACE2 (120 – 135 kDa) protein expression in *Gipr*$^{+/+}$, *Gipr*$^{-/-}$, and *Gipr*$^{-/-}$:MHC-*Lipe* mice hearts (viable myocardium) at 48 hrs post-LAD coronary artery occlusion. M: TAG content in hearts aerobically perfused for 80 min and treated with either PBS or 20 nM DA-GIP at 45 min of perfusion (n = 4-7). N: The percent of radiolabeled palmitate within the myocardial TAG pool at the end of the isolated working heart perfusion (n = 4).Values represent mean ± SE. Differences were determined using an unpaired Student's two-tailed t-test or a 2-way ANOVA followed by a Bonferroni post-hoc analysis. **P*<0.05, significantly different from PBS counterpart.

**Supplementary Table 1.** *In vivo* assessment of cardiac function and LV structure in *Gipr*$^{+/+}$, *Gipr*$^{-/-}$, and *Gipr*$^{-/-}$:MHC-*Lipe* mice following LAD coronary artery ligation surgery. Related to Figure 1 and Figure 3.

| | *Gipr*$^{+/+}$ Pre-MI | *Gipr*$^{+/+}$ Post-MI | *Gipr*$^{-/-}$ Pre-MI | *Gipr*$^{-/-}$ Post-MI | *Gipr*$^{-/-}$:MHC-*Lipe* Pre-MI | *Gipr*$^{-/-}$:MHC-*Lipe* Post-MI |
|---|---|---|---|---|---|---|
| **EF (%)** | 54.6 ± 3.1 | 23.7 ± 2.6* | 57.1 ± 4.1 | 32.9 ± 3.8*$^{\#}$ | 55.1 ± 3.4 | 23.0 ± 3.7* |
| **FS (%)** | 28.0 ± 2.0 | 11.0 ± 1.3* | 30.2 ± 3.0 | 15.9 ± 2.1*$^{\#}$ | 28.5 ± 2.3 | 10.8 ± 1.8* |
| **Heart Rate (BPM)** | 492.1 ± 20.6 | 507.3 ± 19.8 | 478.2 ± 14.8 | 532.3 ± 14.4 | 483.2 ± 34.0 | 508.7 ± 14.6 |
| **LVIDd (mm)** | 4.0 ± 0.1 | 5.0 ± 0.2* | 3.9 ± 0.1 | 4.8 ± 0.1* | 3.9 ± 0.1 | 5.5 ± 0.4* |
| **LVIDs (mm)** | 2.9 ± 0.1 | 4.5 ± 0.2* | 2.8 ± 0.2 | 4.1 ± 0.2* | 2.8 ± 0.1 | 4.9 ± 0.4* |
| **LVAWd (mm)** | 0.88 ± 0.04 | 0.89 ± 0.12 | 0.92 ± 0.02 | 0.92 ± 0.05 | 0.98 ± 0.05 | 0.87 ± 0.11 |
| **LVPWd (mm)** | 0.96 ± 0.05 | 1.04 ± 0.08 | 0.88 ± 0.03 | 0.97 ± 0.05 | 0.98 ± 0.07 | 0.99 ± 0.07 |
| **LVEDV (µL)** | 68.2 ± 4.4 | 120.4 ± 11.0* | 68.0 ± 3.3 | 109.1 ± 7.0*$^{\$}$ | 67.2 ± 4.5 | 153.7 ± 26.0* |
| **LVESV (µL)** | 31.4 ± 3.4 | 92.3 ± 9.1* | 29.8 ± 3.4 | 74.9 ± 8.1*$^{\$}$ | 30.3 ± 3.2 | 124.1 ± 25.9* |

*In vivo* cardiac function and LV wall measurements were assessed via ultrasound echocardiography in isoflurane anesthetized *Gipr*$^{+/+}$, *Gipr*$^{-/-}$, and *Gipr*$^{-/-}$:MHC-*Lipe* mice (n = 6-10). Values represent mean ± SE. $^{*}P<0.05$, indicates a significant difference from pre-MI counterpart. $^{\#}P<0.05$, indicates a significant difference from post-MI *Gipr*$^{+/+}$ and *Gipr*$^{-/-}$:MHC-*Lipe* mice. $^{\$}P<0.05$, indicates a significant difference from post-MI *Gipr*$^{-/-}$:MHC-*Lipe* mice. BPM = beats per minute, d = diastole, EF = ejection fraction, FS = fractional shortening, LV = left ventricular, LVAW = LV anterior wall, LVEDV = LV end diastolic volume, LVESV = LV end systolic volume, LVPW = LV posterior wall, LVID = LV internal diameter, s = systole.

Supplementary Table 2. Corresponding clinical characteristics associated with human heart tissue donors. Related to Supplementary Figure 1.

| Sample | Tissue Source | CHF Etiology | Age (years) | Weight (kg) | Height (cm) | BMI ($kg/m^2$) | BSA (g/dl) | HW (g) | LV Mass (g) | HW Index | Afib | VT/VF | Diabetes | Hypertension | LVEF | Creatinine (mg/dl) |
|---|---|---|---|---|---|---|---|---|---|---|---|---|---|---|---|---|
| 1 | C | ID-CMP | 42 | 115 | 180 | 35.5 | 2.4 | 528 | N/A | 220 | Y | N | N | N | 0.15 | 1 |
| 2 | C | ID-CMP | 62 | 83 | 183 | 24.8 | 2.1 | 662 | N/A | 315 | Y | N | N | N | 0.1 | 1.25 |
| 3 | C | ID-CMP | 65 | 68 | 180 | 21 | 1.8 | 624 | 433 | 347 | N | N | N | N | 0.1 | 1.27 |
| 4 | C | ID-CMP | 42 | 89 | 195 | 23.4 | 2.2 | 744 | 392 | 338 | Y | Y | Y | Y | 0.1 | 1.1 |
| 5 | NF | NF | 51 | 91 | 173 | 30.4 | 2.1 | 286 | 156 | 136 | U | U | Y | U | 0.55 | 0.8 |
| 6 | NF | NF | 69 | 67 | 183 | 20 | 1.8 | 377 | 176 | 209 | N | N | N | Y | U | 1.08 |
| 7 | C | ID-CMP | 54 | 60 | 173 | 20 | 1.7 | 434 | 244 | 255 | N | Y | N | N | 0.15 | 1.29 |
| 8 | NF | NF | 77 | 78 | 170 | 27 | 1.9 | 495 | 181 | 261 | Y | N | N | Y | U | 0.8 |
| 9 | NF | NF | 59 | 132 | 175 | 43.1 | 2.5 | 498 | 234 | 199 | N | N | Y | Y | 0.6 | 0.88 |
| 10 | NF | NF | 51 | 121 | 183 | 36.1 | 2.5 | 516 | 265 | 206 | N | N | N | N | 0.55 | 1.5 |
| 11 | C | ID-CMP | 62 | 86 | 195 | 22.6 | 2.2 | 730 | 395 | 332 | Y | N | N | N | 0.12 | 1.08 |
| 12 | NF | NF | 78 | 92 | 175.3 | 29.9 | 2.1 | 448 | 234 | 213 | N | N | N | Y | U | U |
| 13 | NF | NF | 81 | 78 | 170 | 27 | 1.9 | 402 | 218 | 212 | N | N | N | Y | U | 1.6 |
| 14 | C | ID-CMP | 49 | 76 | 170 | 26.3 | 1.9 | 424 | 269 | 223 | N | N | Y | Y | 0.18 | 0.69 |
| 15 | NF | NF | 22 | 67 | 180 | 20.7 | 1.8 | 299 | 182 | 166 | N | N | N | N | 0.55 | 1 |

All cardiac tissue samples were obtained from male, Caucasian patients. Afib, atrial fibrillation; BMI, body mass index; BSA, blood serum albumin; C, cardiomyopathy; CHF, chronic heart failure; HW; heart weight; ID-CMP, idiopathic cardiomyopathy; LV, left ventricle; LVEF, left ventricular ejection fraction; N, no; NF, non-failing; VT/VF, ventricular tachycardia/ventricular fibrillation; U, unknown; Y, yes.